Copy
RM L9K25a

NACA

RESEARCH MEMORANDUM

PRELIMINARY RESULTS FROM A FREE-FLIGHT INVESTIGATION AT TRANSONIC AND SUPERSONIC SPEEDS OF THE LONGITUDINAL STABILITY AND CONTROL CHARACTERISTICS OF AN AIRPLANE CONFIGURATION WITH A THIN STRAIGHT WING OF ASPECT RATIO 3

By Clarence L. Gillis, Robert F. Peck, and A. James Vitale

Langley Aeronautical Laboratory
Langley Air Force Base, Va.

NATIONAL ADVISORY COMMITTEE FOR AERONAUTICS
WASHINGTON
February 14, 1950

NACA RM L9K25a

NATIONAL ADVISORY COMMITTEE FOR AERONAUTICS

RESEARCH MEMORANDUM

PRELIMINARY RESULTS FROM A FREE-FLIGHT INVESTIGATION AT TRANSONIC AND SUPERSONIC SPEEDS OF THE LONGITUDINAL STABILITY AND CONTROL CHARACTERISTICS OF AN AIRPLANE CONFIGURATION WITH A THIN STRAIGHT WING OF ASPECT RATIO 3

By Clarence L. Gillis, Robert F. Peck, and A. James Vitale

SUMMARY

A flight test at transonic and supersonic speeds was conducted on a rocket-propelled airplane model having a thin straight tapered wing of aspect ratio 3 and hexagonal airfoil sections. Information was obtained on the longitudinal stability and control characteristics of the configuration by analyzing the response of the model to rapid deflections of the horizontal tail. The Mach number range covered in the test was from 0.75 to 1.42. The flying qualities for an assumed full-scale airplane were computed.

The results obtained indicated that some nonlinearity of the lift curves is present at Mach numbers between 0.75 and 1.00. At high subsonic speeds maximum normal-force coefficients of about 0.8 were obtained during abrupt pull-ups. The aerodynamic center varies somewhat erratically with Mach number, first moving forward and then moving rearward, in two steps, a total distance of about 27 percent of the mean aerodynamic chord as the Mach number is increased from subsonic to supersonic speeds. The damping of the short-period longitudinal oscillation (in cycles to damp to one-tenth amplitude) for an assumed full-scale airplane at an altitude of 40,000 feet and supersonic speeds would be rather poor with the center of gravity at 12.4 percent of the mean aerodynamic chord. The maneuverability of the assumed airplane at subsonic speeds and an altitude of 40,000 feet would be seriously limited by the maximum lift coefficient attainable.

INTRODUCTION

A general research program, utilizing rocket-propelled models in free flight, has been initiated by the National Advisory Committee for Aeronautics to study the longitudinal stability and control characteristics of airplane configurations at transonic speeds. Both the static and dynamic stability characteristics are obtained by disturbing the model during flight and studying the resulting motion. The present paper contains the results from the flight of the first model in this program. The model had a straight tapered wing and horizontal tail of aspect ratio 3 with 4.5-percent-thick hexagonal airfoil sections. The Mach number range covered in the test was from 0.75 to 1.42.

An all-movable horizontal tail was used for longitudinal control and during the flight the tail was moved between deflections of $\pm 2^{\circ}$ in approximately a square-wave pattern. The basic aerodynamic parameters of the airplane configuration and the flying qualities for a full-scale airplane were determined from the response of the model to the elevator motion. An analysis of the flight time history was made to obtain the longitudinal stability characteristics for this configuration. The methods of analysis used are described in some detail. The model was flown at the Langley Pilotless Aircraft Research Station, Wallops Island, Va.

SYMBOLS

C_N	normal-force coefficient $\left(\frac{a_n}{g}\frac{W/S}{q}\right)$
C_c	chord-force coefficient $\left(-\frac{a_l}{g}\frac{W/S}{q}\right)$
C_L	lift coefficient $(C_N \cos \alpha - C_c \sin \alpha)$
C_D	drag coefficient $(C_c \cos \alpha + C_N \sin \alpha)$
C_m	pitching-moment coefficient
C_h	hinge-moment coefficient
a_n	normal acceleration, feet per second per second
a_l	longitudinal acceleration, feet per second per second; positive forward

[redacted]

g	acceleration of gravity, feet per second per second
H	total pressure, pounds per square foot
p	free-stream static pressure, pounds per square foot
q	dynamic pressure, pounds per square foot $\left(\frac{\gamma}{2}pM^2\right)$
ρ	atmospheric density, slugs per cubic foot
γ	specific heat ratio, (1.40) $\left(\text{equations for } \frac{H}{p}\right)$
γ	flight-path angle (equation (A15)), degrees
V	velocity, feet per second
V_c	velocity of sound, feet per second
M	Mach number
W	weight, pounds
S	wing area (including the area enclosed within the fuselage), square feet
$\bar{c}$	wing mean aerodynamic chord, feet
α	angle of attack, degrees
δ	elevator deflection, degrees
θ	angle of pitch, degrees
I_Y	moment of inertia about y-axis, slug-feet^2
k	radius of gyration in pitch
m	mass
$I' = \frac{I_Y}{Sq\bar{c}}$	
$m' = \frac{mV}{Sq}$	
$\dot{V} = \frac{dV}{dt}$	

[redacted]

l	tail length; distance from center of gravity to tail aerodynamic center
P	period of oscillation, seconds
t	time, seconds
T_x	time to damp to x fraction of original amplitude, seconds
$c_{1/10}$	cycles required to damp to one-tenth amplitude
ϕ	angle of roll, (equation (A15)), degrees
A,B,C,X,Y,Z,ϕ	constants used in developing equations for analysis
x_{ac}	distance from leading edge of mean aerodynamic chord to aerodynamic center of airplane, percent of mean aerodynamic chord
x_{cg}	distance from leading edge of mean aerodynamic chord to center of gravity of airplane, percent of mean aerodynamic chord

Subscripts:

$\dot{\alpha} = \frac{d\alpha}{dt}\frac{\bar{c}}{2V}$	
T	trim
a	airplane
m	model
$q = \frac{d\theta}{dt}\frac{\bar{c}}{2V}$	
0	value at $\alpha = \delta = 0$

The symbols α, δ, q, and $\dot{\alpha}$ used as subscripts indicate the derivative of the quantity with respect to the subscript, for example

$$C_{N_\alpha} = \frac{dC_N}{d\alpha}$$

[redacted]

MODEL AND APPARATUS

A three-view drawing of the model is shown in figure 1. This was a general research model representing no particular airplane configuration. The fuselage was a body of revolution containing a cylindrical center section and a nose and tail section derived from nose shape of model 9 of reference 1 by increasing the nose fineness ratio. The ordinates of the nose and tail sections of the fuselage are given in table I. The fuselage was not an optimum aerodynamic shape but was selected from considerations of ease of fabrication, adaptability for altering fuselage shape and internal arrangement, and of minimizing wing-fuselage interference changes when changing wing location or plan form (see reference 2). Since major changes in wing plan form, size, and location are contemplated in a general research program, the vertical tail was designed to provide a fairly large reserve margin of directional stability.

The wing used on the model described herein had a 4.5-percent-thick hexagonal airfoil section as shown in figure 1 and was made of solid steel. The amount of sweepback incorporated (16° at the quarter-chord line) was selected from aeroelastic considerations. Since the aerodynamic effect of this amount of sweep would be very small, the wing is considered to be unswept for purposes of discussion and comparison with other results. Photographs of the model are shown in figure 2.

The solid duralumin horizontal tail was identical to the wing in plan form and section and was mounted on a ball bearing built into the vertical tail (fig. 3). The tail hinge line was at 42 percent of the tail mean aerodynamic chord. During the flight the tail was operated as an elevator by an electric motor between deflections of ±2° in approximately a square-wave pattern. The horizontal tail was placed in a rather high position to minimize trim changes due to downwash changes in the transonic region.

For this test the weight of the model was 126 pounds, the pitching moment of inertia was 8.91 slug-feet squared, and the center of gravity was at 12.4 percent of the mean aerodynamic chord.

The model contained a six-channel telemeter. The measurements made were normal and longitudinal acceleration, elevator deflection, angle of attack, total pressure, and a reference static pressure for determining Mach number and dynamic pressure. The angle of attack was measured by a vane-type instrument located on the nose of the model (fig. 2) which is more fully described in reference 3. The total-pressure tube was located on a small strut below the fuselage. Previous flights of instrumentation test models had shown that this location caused no measurable total-pressure errors.

[redacted]

A Doppler radar unit was available for measuring the velocity of the model and a tracking radar was available for obtaining range and elevation as a function of time. Atmospheric conditions were determined from a radiosonde released at the time of firing. Fixed and manually operated 16-millimeter motion-picture cameras were used to observe the launching and the first part of the flight.

The model was boosted to a Mach number of 1.42 by a 6-inch-diameter dry-fuel Deacon rocket motor and was then separated from the booster by reason of the different drag-weight ratios of the model and booster. The model itself contained no rocket.

For launching, the model was attached to the front of the booster as a cantilever (fig. 4) by means of the cone-shaped end of the model (fig. 1). The booster was supported on a crutch-type launcher as shown in figure 4. The launching angle was 44.5°.

TEST AND ANALYSIS PROCEDURES

Test

All of the data were obtained during the decelerating part of the flight following separation of the model and booster. An electrical power unit within the model operated the elevator between deflections of approximately ±2° in a continuous square-wave program at a rate of about 1 cycle per second. Figure 5 shows typical portions of the time histories of normal-force coefficient, angle of attack, elevator deflection, and Mach number obtained during the flight. The small breaks in the elevator deflection curves (fig. 5(b)) indicate that the elevator is moving off the stop slightly under the action of the aerodynamic hinge moment.

The Doppler radar and tracking radar obtained information during the boosted part of the flight but failed to track the model after separation from the booster. The Mach numbers and dynamic pressures during decelerating flight were therefore calculated entirely from the telemetered total pressure and static pressure. The Doppler radar velocity obtained furnished a check on the Mach numbers from telemetered measurements during the accelerating part of the flight and at peak velocity.

The Mach number was computed from the following relations:

subsonic

$$\frac{H}{p} = \left(1 + \frac{\gamma - 1}{2} M^2\right)^{\frac{\gamma}{\gamma-1}}$$

supersonic

$$\frac{H}{p} = \frac{\left(\frac{\gamma + 1}{2} M^2\right)^{\frac{\gamma}{\gamma-1}}}{\left(\frac{2\gamma}{\gamma + 1} M^2 - \frac{\gamma - 1}{\gamma + 1}\right)^{\frac{1}{\gamma-1}}}$$

where H was measured by the total-pressure tube underneath the model (fig. 1) and p was obtained from the reference static-pressure measurement. The static-pressure measurement used had been calibrated on previous flights of instrumentation test models.

The angles of attack measured by the vane on the nose of the model were corrected to angles at the model center of gravity by the method of reference 3.

The Reynolds numbers obtained during this flight are shown in figure 6 as a function of Mach number.

Accuracy

It is impossible to state precisely the limits of accuracy of each quantity derived from free-flight model tests. Tests of identical models probably furnish the best check on the accuracy of the results. The probable accuracy of the various aerodynamic derivatives derived from the test results depends on how they are determined (see appendix A).

In general the absolute value of any telemetered measurement can be in error by 2 percent of the total calibrated instrument range. The Doppler radar velocity is known to be accurate to better than 1 percent for nonmaneuvering models. The Mach number at peak velocity should therefore be accurate to 1 percent or better. Since the Mach number subsequent to peak velocity was determined from telemetered data, it probably becomes less accurate as the Mach number decreases. Since the dynamic pressure is proportional to the Mach number squared, its probable inaccuracy is approximately twice that of the Mach number.

[redacted]

Quantities such as C_{L_α} and C_D are subject to the most error because they depend on the measured normal and longitudinal accelerations and the dynamic pressure. The quantity C_{m_α} is determined from the period of an oscillation and will thus be unaffected by the accuracy of the measured values of angle of attack or normal acceleration. It will depend on the accuracy of the dynamic pressure, the timing marks on the telemeter record, and the preflight determination of the model moment of inertia. Since the aerodynamic-center location depends on the ratio $C_{m_\alpha}/C_{L_\alpha}$ it should be unaffected by errors in determining dynamic pressure. Values of α and δ and quantities determined from them are of course also unaffected by dynamic pressure errors.

Analysis

After each elevator deflection the model experienced a short-period oscillation as shown in figure 5. These oscillations were analyzed to obtain the longitudinal aerodynamic derivatives for the configuration tested and the flying qualities for an assumed full-size airplane. The methods of analysis used are discussed in appendix A. Appendix B presents the results of a study made to investigate the effect on the results of the assumptions made in the analysis.

RESULTS AND DISCUSSION

As can be seen from figure 5(b), the time interval during which the stabilizer remained in a fixed position was not sufficient at subsonic speeds to permit more than about one cycle of oscillation to occur. The period of the oscillation and the variation of lift with angle of attack could be determined, but no damping or trim data could be obtained at Mach numbers less than 1.05. The stops on the angle-of-attack vane were set at approximately $\pm 10^\circ$ and at subsonic speeds the angle of attack exceeded this value for a short time during the first cycle of oscillation following a negative stabilizer deflection (fig. 5(b)). The normal acceleration during the same time interval shows an unsymmetrical character while the angle of attack oscillated in a fairly regular sine wave motion. As will be shown subsequently, this indicates a probable stalling of the model. The small abrupt changes in stabilizer deflection during the time it was supposed to remain fixed amounted to about 0.25° and should have only a small effect on the motion (see appendix A). The rate of deflection of the elevator in a positive direction was different from that in the negative direction, as shown in figure 5. The two rates of control deflection were used to determine their relative desirability for test and analysis purposes. The faster control motion

gave a larger amplitude of oscillation which permitted more accurate lift-curve slopes to be determined but did not give as good trim data. The period of the oscillation could be determined about equally well from either amplitude. The rate of control deflection used should be selected on the basis of the information required from the tests.

The data presented herein were obtained from the complete flight time histories by the methods discussed in appendix A. All data presented are for the center of gravity at 12.4 percent of the mean aerodynamic chord.

Basic Aerodynamic Parameters

Lift-curve slope.- The variation of normal-force coefficient with angle of attack and with elevator deflection is shown in figure 7 as a function of Mach number. Although angle-of-attack and chord-force data were available, the normal-force data were not computed as lift coefficients because the difference is very small for the angles of attack obtained and considerable computing time was thereby saved. The values of C_{L_α} would be smaller than C_{N_α} by about 1 percent at Mach numbers above 1.0 and by a smaller amount at Mach numbers less than 1.0.

The data indicate some nonlinearity of the lift curves in the region from $M = 0.75$ to $M = 1.0$ as evidenced by the different slopes obtained for normal-force coefficients in the regions of $C_N = 0$ and 0.4. No values of C_{N_α} could be determined near $C_N = 0$ at supersonic speeds because of the small amplitudes of oscillation following positive elevator deflections. The indications are that the nonlinearity disappears at Mach numbers above 1.0 (fig. 7).

Values of C_{N_δ} calculated by the three methods listed in appendix A are indicated by the three sets of symbols in figure 7. The values of C_{N_δ} are fairly small for this configuration and consequently considerable scatter of the data is evident. Since equations (15) and (16) of appendix A require trim data they could not be used below $M = 1.05$. Equation (14) did not give reliable data below $M = 1.00$ because of the nonlinear character of the curves of C_N against α.

Maximum lift coefficient.- At Mach numbers below 0.95 the model apparently stalled each time it oscillated to a positive angle of attack following a negative control deflection. A typical plot of C_N against α at a subsonic Mach number is shown in figure 8(a). A similar plot at a supersonic Mach number is shown in figure 8(b) for comparison. The data points shown are the points actually reduced from the telemeter

[redacted]

record. The data were recorded continuously, of course, and any number of points could have been obtained.

As shown in figure 8(a), the variation of C_N with α is linear up to a C_N of about 0.6 as the angle of attack increased following control deflection. Above $C_N = 0.6$ the curve became nonlinear and the indications are that the model reached a stalled attitude. The telemeter record indicated a small high-frequency vibration in the nonlinear portion of the curve. When the model decreased angle of attack following the stall it did not follow the same curve of C_N against α. The latter effect has been observed in wind-tunnel and wing-flow tests.

Figure 9 shows the maximum normal-force coefficients obtained during those oscillations in which the model was apparently stalled. Also given in the figure are several values of the rate of change of angle of attack preceding maximum lift. These maximum normal-force coefficients were, of course, obtained under dynamic conditions and are not necessarily the same as would be obtained during static tests. Data in reference 4 show that the maximum lift coefficient obtained in flight increases as the rate of pitch preceding maximum lift increases. The maximum rates of pitch obtained in reference 4 in terms of the nondimensional factor $\frac{d\alpha}{dt}\frac{\bar{c}}{2V}$ used herein were about 0.25. Unpublished results of other similar tests indicate that this dynamic effect on maximum lift decreases as the Mach number increases and probably disappears at high-subsonic Mach numbers. The unpublished data referred to and the data in reference 4 are for airplanes with conventional round-nose airfoils. Conclusions drawn from such tests may or may not be applicable to sharp-nose hexagonal airfoils such as those used on the model described herein.

Aerodynamic-center location.- The measured periods of oscillation of the angle of attack are used to determine the static stability. The periods are shown in figure 10(a) and the data converted to aerodynamic-center location are shown in figure 10(b). The measured oscillation periods indicate some nonlinearity in the pitching-moment curves at subsonic speeds. The curve faired through the data for negative control deflections at subsonic speeds has been dotted to indicate those periods which were obtained from the oscillations in which the angle-of-attack vane was against a stop during part of the oscillation. As the Mach number is increased above about 0.82 the aerodynamic center first moves forward to its most forward location of 35 percent of the mean aerodynamic chord at a Mach number of 0.90. It then moves rearward between Mach numbers of 0.90 and 1.0, remains fairly constant to a Mach number of 1.15, and then moves rearward again to the most rearward location of 62 percent of the mean aerodynamic chord at a Mach number of 1.30.

[redacted]

Damping in pitch.- The time required for the oscillations of the model to damp to one-half amplitude is shown in figure 11(a) and the data converted to the damping factor $\left(C_{m_q} + C_{m_{\dot{\alpha}}}\right)$ are given in figure 11(b). Although the decrease in $\left(C_{m_q} + C_{m_{\dot{\alpha}}}\right)$ with increasing Mach number above $M = 1.05$ appears to be excessive, it is of the right order of magnitude when compared with estimated values.

Drag.- The minimum drag coefficients obtained from this flight are shown in figure 12. The longitudinal accelerometer in this model was calibrated to cover a sufficient range to include the accelerations during booster burning (about 18g) and thus did not give very good accuracy on the accelerations (about -1g to -4g) developed during the time the drag data were obtained. This is evidenced by the scatter of data in figure 12.

The drag at supersonic speeds is fairly high and is due mostly to the fuselage which is not a particularly good shape for supersonic speeds, as mentioned previously.

The effect of lift on drag is shown in various ways in figures 13 and 14. The $\left(\frac{C_N}{C_D}\right)_{max}$ decreases by about one-half as the Mach number increases from 0.8 to 1.0. This decrease is apparently due to the increase in minimum drag because $\frac{dC_D}{dC_N{}^2}$ does not increase in this Mach number region, as shown in figure 13. The dashed curve in figure 13 is a plot of $\frac{1}{57.3C_{N_\alpha}}$ which should equal the value of $\frac{dC_D}{dC_N{}^2}$ for a wing with the resultant force normal to the chord plane. The agreement between this curve and the measured values of $\frac{dC_D}{dC_N{}^2}$ is good except at the highest Mach numbers. The rather large value of $\frac{dC_D}{dC_N{}^2}$ at a Mach number of 1.35 is in accord with the results of reference 5 which gives a value of about 0.3 for a straight wing of aspect ratio 4 at a Mach number of 1.53.

Longitudinal trim and control effectiveness.- Curves of trim normal-force coefficient and trim angles of attack are shown in figure 15 for elevator deflections of $\pm 2.0^\circ$. The magnitude of the trim change through the transonic region cannot be determined from the data, but the indications from the telemeter record are that any such trim changes were small. It is interesting to note that in the supersonic region covered by the

test a stabilizer deflection of 2° trims the model at approximately zero angle of attack and zero lift. This indicates that at zero lift a downflow angle of approximately 2° probably existed at the horizontal tail. The value of C_{m_o} in the supersonic region covered was calculated to be approximately 0.095. The downflow angle is probably caused mostly by the converging flow over the rear portion of the fuselage with possibly a small effect due to inflow into the wing wake. In addition, the drag of the tail surfaces would cause a positive pitching moment.

Although no values of trim lift or angle of attack could be obtained below $M = 1.05$, the amplitudes of motion indicated that the control effectiveness was maintained in the transonic region. The values of C_{m_δ} are shown in figure 16.

Airplane Flying Qualities

The data have been also analyzed in terms of some of the important flying-quality items for an assumed airplane at an altitude of 40,000 feet and having the characteristics enumerated in table II. An airplane having a wing like that tested on the rocket model would necessarily carry all, or nearly all, of the fuel in the fuselage, which accounts for the rather large value of moment of inertia given in table II.

Longitudinal trim and control effectiveness.- Elevator deflections for trim for level flight are shown in figure 17. The control effectiveness in terms of normal accelerations in g produced by a one-degree change in elevator deflection is shown in figure 18.

As mentioned in appendix A, corrections to the trim elevator deflections were made to account for the model not being in straight level flight when the trim deflections were determined. Calculations showed that for the trim condition in figure 17 the correction never exceeded 0.02° of elevator deflection.

Dynamic stability.- The period and damping of the short-period longitudinal oscillation for the assumed airplane are shown in figure 19. The damping of the oscillation, in the region where damping data could be determined, was not very good when judged by the usual criterion of cycles to damp to one-tenth amplitude. In one cycle the oscillation damped to about one-half amplitude compared to the desired value of one-tenth. One of the reasons for the relatively poor damping is the large moment of inertia. Another reason is the fairly large static margin used on the model. The damping, in terms of cycles required to damp to one-tenth amplitude, would become better as the center of gravity is moved rearward. Also, of course, the damping would be better at lower altitudes.

[redacted]

Maximum normal acceleration.- The values of maximum normal acceleration that could be developed on the assumed airplane in the Mach number region where the model was apparently stalled are shown in figure 20. It is evident that very little maneuverability is available at subsonic speeds at an altitude of 40,000 feet, and the airplane could not be maintained in level flight at 40,000 feet below M = 0.73 unless a high-lift device of some kind were used.

General Remarks

The test technique used involves measuring some of the aerodynamic derivatives while the model is oscillating. Analytical investigations such as references 6, 7, and 8 show that the oscillation frequency has an effect on the aerodynamic derivatives. For the analysis contained in this paper no calculations have been made of the effect of oscillation frequency on the results. The aerodynamic derivatives for a full-scale airplane would also be affected by such oscillating motion, so for calculating the response of the airplane the derivatives contained herein are more nearly applicable than those obtained under essentially steady flow conditions. If the rocket model were dynamically similar to the full-scale airplane, no corrections to the data for transient effects would be necessary. If it is desired to compute such corrections, the oscillation periods in figure 10 may be used to determine the frequency.

CONCLUSIONS

A flight test at transonic and supersonic speeds of a rocket-propelled airplane model having a thin straight wing of aspect ratio 3 and hexagonal airfoil section indicated the following conclusions:

1. No large or abrupt changes in lift-curve slope occurred in the Mach number range covered (0.75 to 1.42), but evidence of some nonlinearity in the lift curves was obtained at Mach numbers between 0.75 and 1.00.

2. The model apparently stalled at Mach numbers below 0.95 following abrupt control deflection. The maximum dynamic normal-force coefficients obtained were about 0.8.

3. The aerodynamic-center location varied with lift coefficient in the subsonic region but showed no variation with lift coefficient at supersonic speeds within the range tested. The most forward aerodynamic-center location of 35 percent of the mean aerodynamic chord occurred at a Mach number of 0.90 and the most rearward location of 62 percent occurred at a Mach number of 1.30.

[redacted]

4. The drag coefficients are fairly large at supersonic speeds, probably due to the fuselage shape.

5. The damping of the short-period longitudinal oscillation (in cycles to damp to one-tenth amplitude) for an assumed full-scale airplane at an altitude of 40,000 feet would be fairly poor at supersonic speeds with a center-of-gravity location at 12.4 percent of the mean aerodynamic chord. The damping time (in number of cycles) would improve if the center of gravity were moved rearward.

6. The maneuverability of a full-scale airplane at subsonic speeds at an altitude of 40,000 feet would be seriously limited by the maximum lift coefficient attainable.

Langley Aeronautical Laboratory
National Advisory Committee for Aeronautics
Langley Air Force Base, Va.

[redacted]

APPENDIX A

Method of Analysis

The method of analysis used herein applies to the free oscillation resulting from a step-function disturbance. The complete derivation of the equations used will not be given herein because it is fairly simple and may be found in a number of sources. Only the final results and the method of applying them to free-flight models will be shown. The discussion has been kept general in character for purposes of application to other models. Some of the procedures discussed are not directly applicable to the particular model discussed in the main body of the paper.

In order to simplify the analysis and to permit the determination of equations for the more important aerodynamic derivatives, several assumptions are necessary. It is assumed that during the time interval over which each calculation is made, the following conditions hold: the forward velocity and Mach number are constant; the aerodynamic forces and moments vary linearly with α, θ, δ, $\frac{d\alpha}{dt}$, and $\frac{d\theta}{dt}$; and the model is in level flight before the disturbance is applied. A discussion of the effect of these assumptions upon the results will be found in appendix B.

The first assumption mentioned in the previous paragraph effectively limits the longitudinal disturbed motion of the aircraft to two degrees of freedom: translation normal to the flight path and rotation in pitch about the center of gravity. The equations of motion resulting from these assumptions are

θ: pitch angle
α: angle of attack
δ: elevator deflection

$$m'\frac{1}{57.3}\left(\frac{d\theta}{dt} - \frac{d\alpha}{dt}\right) = C_{L_\alpha}\alpha + C_{L_\delta}\delta \tag{A1}$$

$$I'\left(\frac{1}{57.3}\right)\frac{d^2\theta}{dt^2} = C_{m_\alpha}\alpha + C_{m_{\dot{\alpha}}}\left(\frac{\bar{c}}{2V}\right)\frac{d\alpha}{dt} + C_{M_q}\left(\frac{\bar{c}}{2V}\right)\frac{d\theta}{dt} + C_{M_\delta}\delta \tag{A2}$$

When these equations are solved the following equation for the free oscillation of the angle of attack is obtained:

$$\alpha = Ce^{At}\cos(Bt + \phi) + \alpha_T \tag{A3}$$

[redacted]

The α_T is the steady state or trim angle of attack which will exist after the oscillation has damped out and is the mean value about which the angle of attack oscillates. The first term represents the oscillation about the trim angle. Figure 21 is a schematic plot showing a typical record of the angle-of-attack response following a step deflection of the aircraft control surface.

The constants A, B, and α_T in equation (A3) are independent of the initial conditions and the analysis consists essentially of finding the numerical values of these constants from the measured data and from them determining the aerodynamic characteristics of the configuration tested. The constants C and ϕ depend upon the initial conditions and are not used in the analysis, so their numerical values need not be known for the type of analysis considered herein.

From the envelope curves enclosing the oscillations the damping constant A can be determined. If the notation in figure 21 is referred to,

$$\Delta\alpha_2 = \Delta\alpha_1 e^{A(t_2-t_1)}$$

$$A = \frac{\log_e \frac{\Delta\alpha_2}{\Delta\alpha_1}}{t_2 - t_1} \tag{A4}$$

The constant B defines the frequency or period of the oscillation and is given by

$$B = \frac{2\pi}{P} \tag{A5}$$

The constant α_T is simply the value of α after the oscillation has damped to a steady value or is the value of α on the mean line of the oscillation as shown in figure 21.

In order to determine the constants A, B, and α_T from the measured data, it is necessary first to fair envelope curves for the oscillation which should be logarithmic curves according to equation (A3). The mean line between the two envelope curves is drawn and values of α_2, α_1, P, and α_T can then be determined and A and B can be calculated.

The success of this procedure depends in part upon the oscillations being rather lightly damped so that several cycles are available during

[redacted]

each oscillation to permit the fairing of envelope curves. If the oscillations are heavily damped, other methods of analysis will be necessary.

The analytical solution of equations (A1) and (A2), which include those aerodynamic derivatives which previous experience has indicated have an important influence on the motion, shows that the constants A and B are given by

$$A = -\frac{57.3}{2}\left[\frac{C_{L_\alpha}}{m'} - \left(C_{m_q} + C_{m_{\dot{\alpha}}}\right)\frac{\bar{c}}{2VI'}\right] \tag{A6}$$

or

$$A = -\frac{57.3}{2}\frac{1}{m'}\left[C_{L_\alpha} - \left(C_{m_q} + C_{m_{\dot{\alpha}}}\right)\frac{1}{2}\left(\frac{\bar{c}}{k}\right)^2\right] \tag{A7}$$

$$B = \sqrt{57.3\left(\frac{-C_{m_\alpha}}{I'}\right) - (57.3)^2\frac{\bar{c}}{2V}\left(\frac{C_{m_q}C_{L_\alpha}}{I'm'}\right) - A^2} \tag{A8}$$

Probably the most important aerodynamic derivatives that have been omitted from this analysis are C_{L_q} and $C_{L_{\dot{\alpha}}}$. The effect of these and the other omitted terms upon the results is also discussed in appendix B. Solving the steady-state equations will give for α_T

$$\alpha_T = -\frac{C_{m_Q}}{C_{m_\alpha}S} - \frac{C_{m_\delta}}{C_{m_\alpha}}\delta \tag{A9}$$

or

$$\alpha_T = \alpha_{T_{\delta=0}} + \frac{d\alpha_T}{d\delta}\delta \tag{A10}$$

Equations (A6) and (A8) may be rearranged to give

$$\left(C_{m_q} + C_{m_{\dot{\alpha}}}\right) = \frac{4I'V}{57.3\bar{c}}\left(A + \frac{57.3C_{L_\alpha}}{2m'}\right) \tag{A11}$$

$$C_{m_\alpha} = -\frac{I'}{57.3}\left(B^2 + A^2\right) - 57.3\,\frac{\bar{c}}{2V}\,\frac{C_{m_q}C_{L_\alpha}}{m'} \qquad (A12)$$

It is necessary therefore to know the value of C_{L_α} and C_{m_q} to use in equations (All) and (A12) for calculating static stability and damping. It is not possible to separate the terms C_{m_q} and $C_{m_{\dot{\alpha}}}$ when a test procedure measuring only angle of attack and normal acceleration is used. The factor calculated from equation (All) is the total damping coefficient of the configuration, however, and is the quantity desired when estimating the dynamic stability of a full-scale airplane or missile. Numerical calculations have shown that the last term in equation (A12) will probably always be very small compared to the first term (less than 1 percent) and may thus be omitted. Its effect may be estimated in any case. If this term is omitted, the static stability parameter is then

$$C_{m_\alpha} = -\frac{I'}{57.3}\left(B^2 + A^2\right) \qquad (A13)$$

The lift-curve slope C_{L_α} for use in equation (All) is found by plotting C_L against α as obtained from the flight records during an oscillation with the control surface in a fixed position and graphically measuring the slope. A typical plot will look like those shown in figure 8. Another method of determining C_{L_α} is to divide the measured instantaneous slopes $\frac{dC_L}{dt}$ and $\frac{d\alpha}{dt}$ at a given Mach number.

From C_{L_α}, A, B, and the mass characteristics of the model, the damping factor $C_{m_q} + C_{m_{\dot{\alpha}}}$ and the static stability derivative C_{m_α} can be calculated by use of equations (All) and (A13). The aerodynamic-center location for the configuration is then

$$x_{ac} = x_{cg} - \frac{C_{m_\alpha}}{C_{L_\alpha}}\,100 \qquad (A14)$$

The trim characteristics of the configuration are determined from equation (A10). A plot may be made of the values of α_T and δ against Mach number and curves faired through the data. The slope $\frac{d\alpha_T}{d\delta}$ is

[redacted]

obtained from the increments between the curves, and $\alpha_{T_{\delta=0}}$ is obtained by interpolation between the two α_T curves. As can be seen from equations (A9) and (A10), it is now possible to calculate C_{m_o} and C_{m_δ}.

The term "trim" has been used herein to indicate a steady-state condition in which the model is flying with zero aerodynamic pitching moment but in general is not in straight level flight. When calculating airplane stabilizer settings for level-flight trim and for maneuvering, corrections should be applied to the stabilizer deflections determined from the model data to account for the difference in flight-path curvature between the model and airplane at the same lift coefficient. The equation for the increment of control-surface deflection resulting from flight-path curvature is

$$\Delta\delta = 57.3 \frac{C_{m_q}}{C_{m_\delta}} \frac{\bar{c}g}{2V^2}\left(\frac{a_n}{g} - \cos\gamma \cos\phi\right) \tag{A15}$$

In general the roll angle ϕ will not be known for the rocket model. If the model wing loading is relatively small, the second term in equation (A15) will be small compared to the first term, however, and to a first approximation may be neglected.

Several procedures may now be used to determine C_{L_δ}. The value of C_{L_δ} can be obtained from the increment in C_L at any given angle of attack between the lift curves plotted for two successive oscillations at different control deflections. In equation form,

$$C_{L_\delta} = \frac{(\Delta C_L)_{\alpha=\text{Constant}}}{\Delta\delta} \tag{A16}$$

In addition C_{L_δ} can be calculated from the equation

$$C_{L_\delta} = -C_{L_\alpha} \frac{d\alpha_T}{d\delta} + \frac{dC_{L_T}}{d\delta} \tag{A17}$$

where $\frac{dC_{L_T}}{d\delta}$ is found from the C_{L_T} and δ curves in the same manner as $\frac{d\alpha_T}{d\delta}$. Another check on the value of C_{L_δ} can be obtained from

$$C_{L_\delta} = -\frac{C_{m_\delta}}{l/c} \tag{A18}$$

[redacted]

where l/c is the longitudinal distance from the center of gravity to the center of pressure of the lift caused by control-surface deflection. For a conventional airplane configuration with a horizontal tail this distance can be estimated fairly accurately.

The angle of zero lift can also be determined, of course, from the plotted curves of C_L against α.

Although during the tests it is intended that the elevator remain fixed following a deflection, this may not be true because of flexibility in the operating mechanism. If the movement of the control is not so large as to alter significantly the free oscillation, the data may be corrected for the control movement. If the control movement occurs as a sharp break as in figure 5, the lift coefficients can be corrected to a constant-control deflection by the use of the values of C_{L_δ} already determined. New values of C_{L_α} and C_{L_δ} can then be obtained if the change is appreciable. The period and damping constants should be determined before, or after, such breaks in the control-position curve occur but not for a time interval which includes the break. If the control movement occurs as a sinusoidal oscillation in phase with the angle of attack (as in reference 9), the lift coefficients may be corrected as described previously or the correction to C_{L_α} can be found from

$$\Delta C_{L_\alpha} = -C_{L_\delta} \frac{d\delta}{d\alpha} \tag{A19}$$

The correction to C_{m_α} is given by

$$\Delta C_{m_\alpha} = -C_{m_\delta} \frac{d\delta}{d\alpha} \tag{A20}$$

where $\frac{d\delta}{d\alpha}$ is measured directly from the flight time history.

When hinge moments are measured on the model control surface the hinge moment coefficients are plotted against angle of attack for each oscillation similar to the lift coefficients. The slope of the resulting curve gives the parameter C_{h_α}, the vertical displacement between the curves for two successive oscillations at different control deflections gives C_{h_δ}, and interpolation between the two curves yields C_{h_o}, the hinge-moment coefficient at zero angle of attack and control deflection.

In addition to the basic aerodynamic design parameters the flight-test results may be analyzed to obtain the flying qualities for a

[redacted]

full-scale airplane. For this purpose it is not necessary to determine all of the aerodynamic derivatives for the configuration tested unless the flying qualities are desired for a different center-of-gravity location from that on the model tested.

From the curves of C_{L_T} for given control deflections the control deflections for trim can be determined for any airplane flight condition by calculating the lift coefficient required and interpolating from the measured data. Similarly, values of control effectiveness $\frac{\Delta a_n/g}{\Delta\delta}$ can be computed from the same curves. If hinge moments have been measured, the control forces for trim and maneuvering can be calculated.

The period and damping of the longitudinal oscillation for a full-size airplane may be calculated from the model values by the use of the known flight conditions and mass characteristics of each. For this purpose only the lift-curve slope C_{L_α} need be determined from the data or estimated. From equations (A5) and (A13), omitting the A^2 term, the following equation can be derived:

$$P = \frac{2\pi}{\sqrt{\frac{-57.3C_{m_\alpha}}{I'}}} \tag{A21}$$

The A^2 term in equation (A13) is ordinarily only a few percent of the B^2 term and for the purpose of converting from model to airplane values of period its omission is justified. For the same center-of-gravity locations then $C_{m_{\alpha_a}} = C_{m_{\alpha_m}}$ and

$$\frac{P_a}{P_m} = \sqrt{\frac{\rho_m S_m \bar{c}_m}{\rho_a S_a \bar{c}_a} \frac{I_{Y_a}}{I_{Y_m}}} \tag{A22}$$

Similarly, from equations (A4) and (A6) the following equation can be derived for the damping:

$$\frac{\log_e x_a}{T_{x_a}} = \frac{\rho_a S_a \bar{c}_a^2}{\rho_m S_m \bar{c}_m^2} \frac{I_{Y_m} V_{c_m}}{I_{Y_a} V_{c_a}} \frac{\log_e x_m}{T_{x_m}} + 57.3 \frac{C_{L_\alpha} \gamma \rho_a S_a M}{4 V_{c_a}} \left(-\frac{1}{m_a} + \frac{\bar{c}_a^2 I_{Y_m}}{\bar{c}_m^2 I_{Y_a} m_m} \right) \tag{A23}$$

where x is the fraction to which the oscillation has damped in the time T_x.

In this equation x_m and x_a need not be the same. For instance, the damping time usually desired for the airplane is the time to damp to one-tenth amplitude $\left(x_a = \frac{1}{10}\right)$, whereas from the model-flight record it may be more convenient to determine the time to damp to one-half amplitude $\left(x_m = \frac{1}{2}\right)$. The usual damping requirement for airplanes is stated in terms of the number of cycles required to damp to one-tenth amplitude and this can be calculated from

$$c_{1/10} = \frac{-2.303}{P\frac{\log_e x_a}{T_{x_a}}} \tag{A24}$$

[redacted]

APPENDIX B

Effect of Assumptions in Analysis

The purpose of this discussion is to justify the assumptions made in the analysis and to investigate the effects of the more important terms omitted from some of the equations in appendix A.

The effects of the third degree of freedom (fore and aft displacement) actually existing during the flight, the initial inclination of the flight path, the omission of the derivative C_{L_q}, and the omission of the term $\frac{C_{m_q} C_{L_\alpha}}{m'}$ in equation (A12) were all investigated by using the aerodynamic derivatives obtained from the model flight and estimated values of C_{L_q} and C_{m_q} to calculate the period and damping of the short-period oscillation of the model for the following three conditions:

1. Two degrees of freedom with an initial flight-path angle of 0°
2. Two degrees of freedom with an initial flight-path angle of 30° (climbing)
3. Three degrees of freedom with an initial flight-path angle of 30°

Comparison of condition 1 with the measured values of period and damping shows the effect of the omitted terms. Comparison of conditions 1 and 2 shows the effect of the initial flight-path angle. Comparison of conditions 2 and 3 shows the effect of the third degree of freedom.

For all three conditions the calculated period and damping of the short-period oscillation at a Mach number of 1.25 were the same as those measured from the flight time history within 1 in the third significant figure, which is well within computational accuracy. For condition 3, a phugoid oscillation was obtained having a period of 263 seconds. The total flight time for which data were analyzed was 16 seconds. Condition 2 gave a slowly divergent flight-path motion in addition to the short-period oscillation.

The variable forward velocity, which was neglected in the analysis, may be considered to have three effects:

1. A small perturbation velocity resulting from the drag terms in the equation describing the third degree of freedom

[redacted]

2. A quasi-steady state, or basic, motion having a constant acceleration

and

3. The effect of an accelerated air flow on the aerodynamic characteristics of the various components of the aircraft.

The first effect listed has already been investigated and found to be insignificant.

The effect of the constant acceleration of the steady state, or basic, motion was investigated in reference 10 using three degrees of freedom. It was shown that the effect of acceleration is to introduce additional terms $\frac{\dot{V}}{V^2}$ into the characteristic equation, the additional terms being additive to the terms involving lift-curve slope, drag, and damping in pitch, as follows:

$$X = \frac{\rho S C_D}{m} + \frac{\dot{V}}{V^2} \tag{B1}$$

$$Y = \frac{\rho S}{2m}\left(C_D + C_{L_\alpha}\right) + \frac{\dot{V}}{V^2} \tag{B2}$$

$$Z = \frac{\rho S \bar{c}^2}{4I_Y} C_{m_q} + \frac{\dot{V}}{V^2} \tag{B3}$$

Calculations made from the data discussed in the body of this paper give the following numerical results:

$$X = \frac{93}{10^6} - \frac{2.2}{10^6}$$

$$Y = \frac{3490}{10^6} - \frac{2.2}{10^6}$$

$$Z = \frac{2840}{10^6} - \frac{2.2}{10^6}$$

[redacted]

Thus, the acceleration has a measurable effect only on the X term. It has already been found that the X term which appears in the equation describing the third degree of freedom has a negligible effect on the short-period oscillation. It may therefore be concluded that the acceleration has a negligible effect on the results derived from the short-period oscillation.

Reference 11 investigates analytically the effect of accelerated air flow on the pressure drag and lift-curve slope of thin wings in the transonic and supersonic speed ranges. The wing is considered as decelerating from supersonic speeds, which is the actual case for the rocket models. The greatest effect occurs at a Mach number of 1.0 where for unaccelerated air flow the aerodynamic quantities are infinite and for decelerating air flow the aerodynamic quantities are finite. Numerical calculations in reference 11 indicate that at $M = 1.02$, for example, the pressure drag of a wedge airfoil and the lift-curve slope of a flat-plate airfoil of the size on the model discussed in this paper would be decreased by 16 percent if the airfoil were decelerating at a rate of 376g. The actual deceleration obtained on the model was about 4g at supersonic speeds. This effect may therefore be considered negligible.

The calculations described previously indicated that the aerodynamic terms and derivatives omitted from the analysis had a negligible effect on the period and damping of the motion, from which the static stability and damping factor were determined. The effect of the derivatives C_{L_q} and $C_{L_{\dot{\alpha}}}$ on the variation of lift coefficient with angle of attack was investigated also, using estimated values for C_{L_q} and $C_{L_{\dot{\alpha}}}$. It was found that the effect on the slope C_{L_α} was not measurable, but that the values of C_L at a given angle of attack were affected by the direction of motion of the model. That is, when the values of C_L were plotted against α during one oscillation the curve obtained when the model was pitching up did not coincide with the curve obtained when the model was pitching down. The curves had the same slope but were displaced in such a direction as to show a phase lead of the lift coefficient compared to the angle of attack. When calculated corrections for the terms C_{L_q} and $C_{L_{\dot{\alpha}}}$ were applied, the curves tended to move together. The curves in figure 8 have been corrected for this effect. The corrections were larger at subsonic speeds than at supersonic speeds.

The method of analysis in appendix A is not strictly valid if the aerodynamic derivatives are not constant at a given Mach number. The major effects of such nonlinearities can be determined, however, by choosing control-surface deflections which cause the model to oscillate over different ranges of angle of attack. This actually occurred on the model flight described in this paper where different values of C_{L_α}

[redacted]

were obtained for positive and negative control deflections in the transonic region. If the aerodynamic derivatives are extremely nonlinear within the region covered by one oscillation, then the values obtained in the analysis are only average values indicative of the trend of the data.

Certain of the derivatives can be nonlinear without seriously affecting the results. For example, the period of the oscillation is almost completely determined by C_{m_α}, all other terms having only a very small influence; thus, nonlinearities in all other derivatives would not appreciably affect the calculated values of C_{m_α}. Considerable judgment is necessary in interpreting the data when evidences of nonlinearities exist and other more laborious methods of analysis may be necessary.

Since the model is decelerating, the Mach number will change during each oscillation and the aerodynamic derivatives will change also. The values obtained in the analysis are thus average values over a small Mach number interval. The effect of the varying Mach number on the calculated results is minimized by determining the required information over the shortest possible time interval. The lift-curve slope can be determined during one-half cycle of an oscillation, for instance. The static-stability derivative C_{m_α} is obtained by measuring each half-period and multiplying by two, plotting the results against Mach number, and making the computations from a faired curve as shown in figure 10. The damping time can also be measured several times during an oscillation and plotted against Mach number. Similarly, the values of C_{L_O}, C_{L_T}, and α_T can be determined for each oscillation, plotted against Mach number, and the quantities α_{L_O}, $\frac{dC_{L_T}}{d\delta}$, $\frac{d\alpha_T}{d\delta}$, and $\alpha_{T_{\delta=0}}$ obtained from faired curves through the points rather than from the increments between measured points at different Mach numbers.

The change in Mach number during one-half cycle of an oscillation on the flight test reported herein was about 0.01 at supersonic speeds and about 0.0035 at subsonic speeds. Thus, unless the aerodynamic parameters vary very rapidly with Mach number, the error involved should be small.

[redacted]

REFERENCES

1. Ferri, Antonio: Supersonic-Tunnel Tests of Projectiles in Germany and Italy. NACA ACR L5H08, 1945.

2. Mathews, Charles W., and Thompson, Jim Rogers: Comparison of the Transonic Drag Characteristics of Two Wing-Body Combinations Differing Only in the Location of the 45° Sweptback Wing. NACA RM L7I01, 1947.

3. Mitchell, Jesse L., and Peck, Robert F.: An NACA Vane-Type Angle-of-Attack Indicator for Use at Subsonic and Supersonic Speeds. NACA RM L9F28a, 1949.

4. Gadeberg, Burnett L.: The Effect of Rate of Change of Angle of Attack on the Maximum Lift Coefficient of a Pursuit Airplane. NACA RM A8I30, 1949.

5. Vincenti, Walter G., Van Dyke, Milton D., and Matteson, Frederick H.: Investigation of Wing Characteristics at a Mach Number of 1.53. II - Swept Wings of Taper Ratio 0.5. NACA RM A8E05, 1948.

6. Statler, I. C.: Dynamic Stability at High Speeds from Unsteady Flow Theory. Preprint no. 187, Inst. Aero. Sci. Inc., Jan. 1949.

7. Miles, John W.: Quasi-Stationary Thin Airfoil Theory. Jour. Aero. Sci. (Readers Forum), vol. 16, no. 7, July 1949, p. 440.

8. Miles, John W.: On Harmonic Motion at Supersonic Speeds. Jour. Aero. Sci. (Readers Forum), vol. 16, no. 6, June 1949, pp. 378-379.

9. Mitcham, Grady L., Stevens, Joseph E., and Norris, Harry P.: Aerodynamic Characteristics and Flying Qualities of a Tailless Triangular-Wing Airplane Configuration As Obtained from Flights of Rocket-Propelled Models at Transonic and Low Supersonic Speeds. NACA RM L9L07, 1949.

10. Hoch, H.: Untersuchungen zur Stabilität der leitstrahlgeführten Flakrakete. FB Nr. 1892/3 Deutsche Luftfahrtforschung (Berlin-Adlershof), 1944.

11. Gardner, C. S., and Ludloff, H. F.: Influence of Acceleration on Aerodynamic Characteristics of Thin Wings in Supersonic and Transonic Flight. Preprint no. 186, Inst. Aero. Sci., Inc., Jan. 1949.

[redacted]

TABLE I

FUSELAGE NOSE AND TAIL ORDINATES

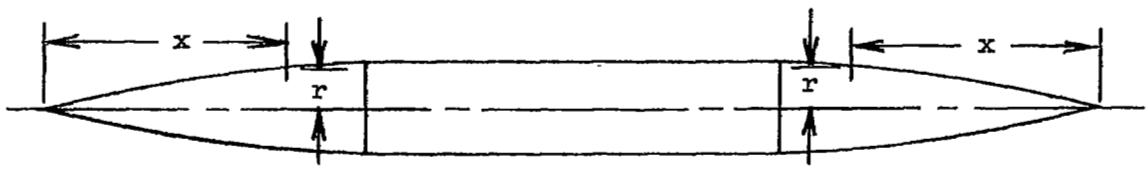

x (in.)	r (in.)
0	0.168
.060	.182
.122	.210
.245	.224
.480	.294
.735	.350
1.225	.462
2.000	.639
2.450	.735
4.800	1.245
7.350	1.721
8.000	1.849
9.800	2.155
12.250	2.505
13.125	2.608
14.375	2.747
14.700	2.785
17.150	3.010
19.600	3.220
22.050	3.385
24.500	3.500

NACA

[redacted]

TABLE II

CHARACTERISTICS OF AIRPLANE

Weight, lb	20,000
Wing area, sq ft	170
Mean aerodynamic chord, ft	8.0
Moment of inertia (I_Y), slug-ft^2	50,000

[redacted]

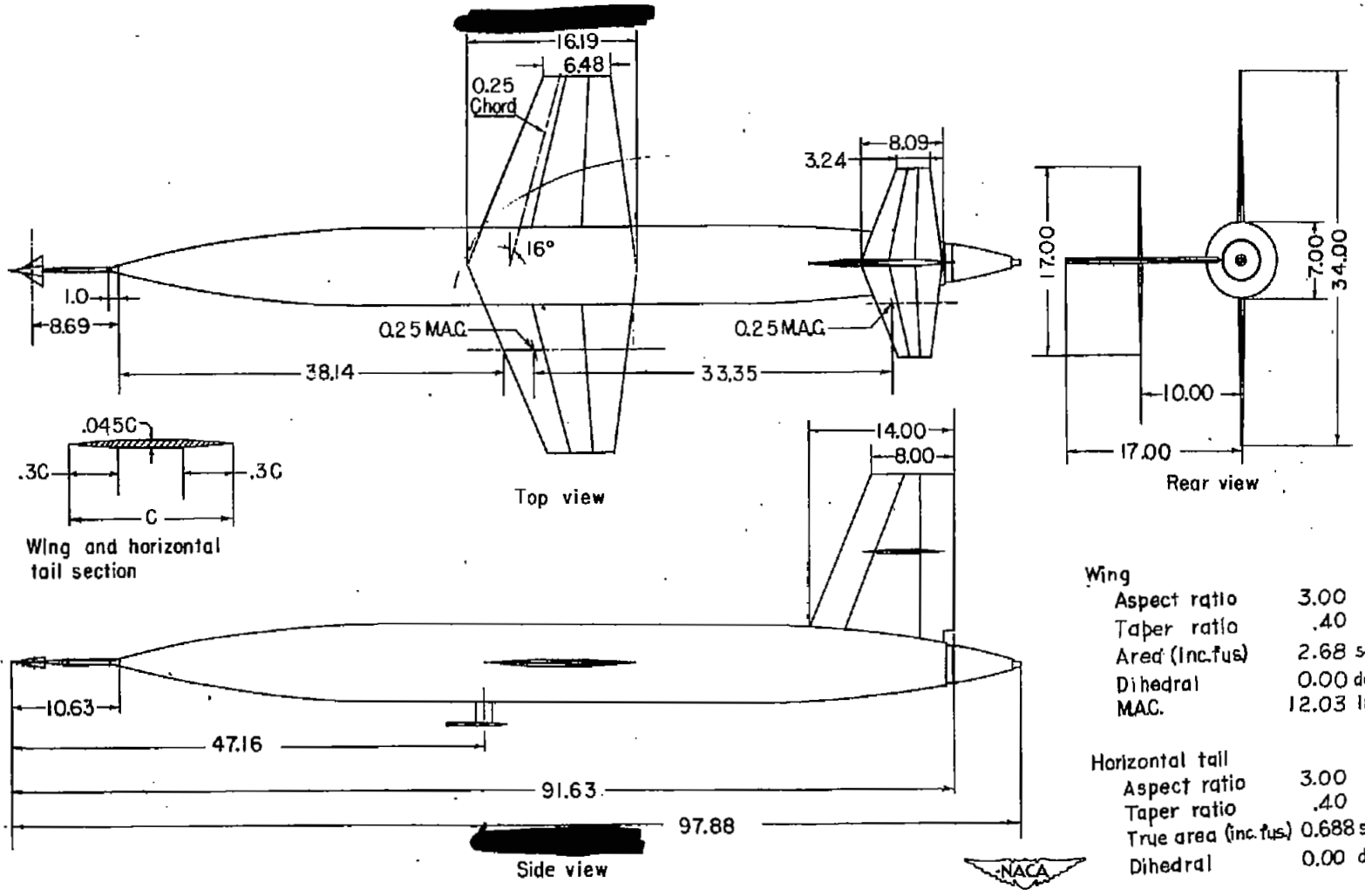

Wing		
Aspect ratio	3.00	
Taper ratio	.40	
Area (inc. fus)	2.68	sq ft
Dihedral	0.00	deg
MAC.	12.03	in.
Horizontal tail		
Aspect ratio	3.00	
Taper ratio	.40	
True area (inc. fus.)	0.688	sq ft
Dihedral	0.00	deg
Vertical tail		
Exposed area	1.11	sq ft

Figure 1.- General arrangement of model. All dimensions in inches.

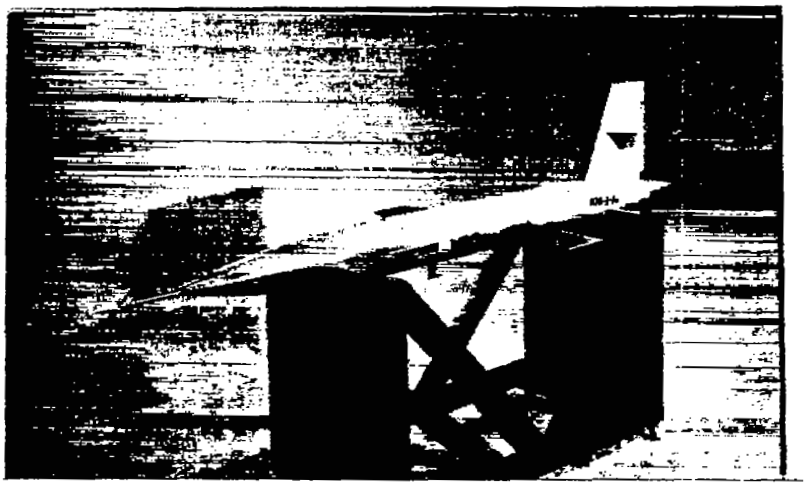

(a) Three-quarter front view.

NACA

L-59511

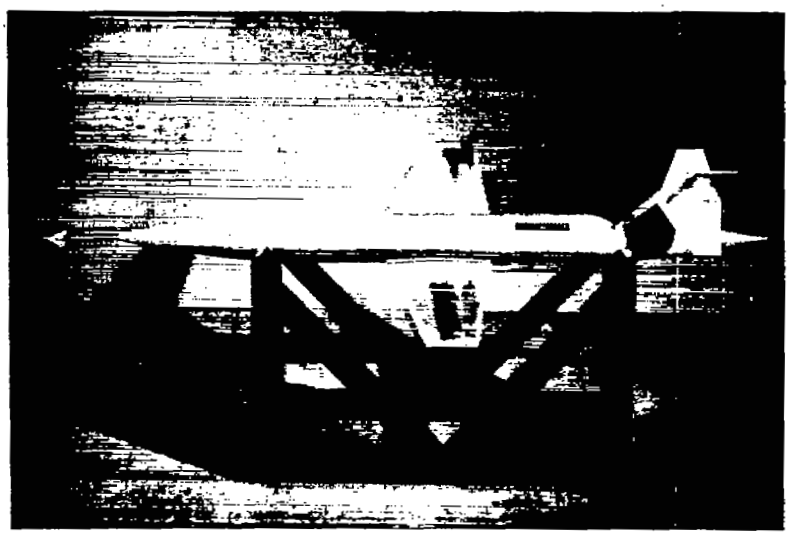

NACA

(b) Top view.

L-59512

Figure 2.- Model tested.

Figure 3.- Tail section of model.

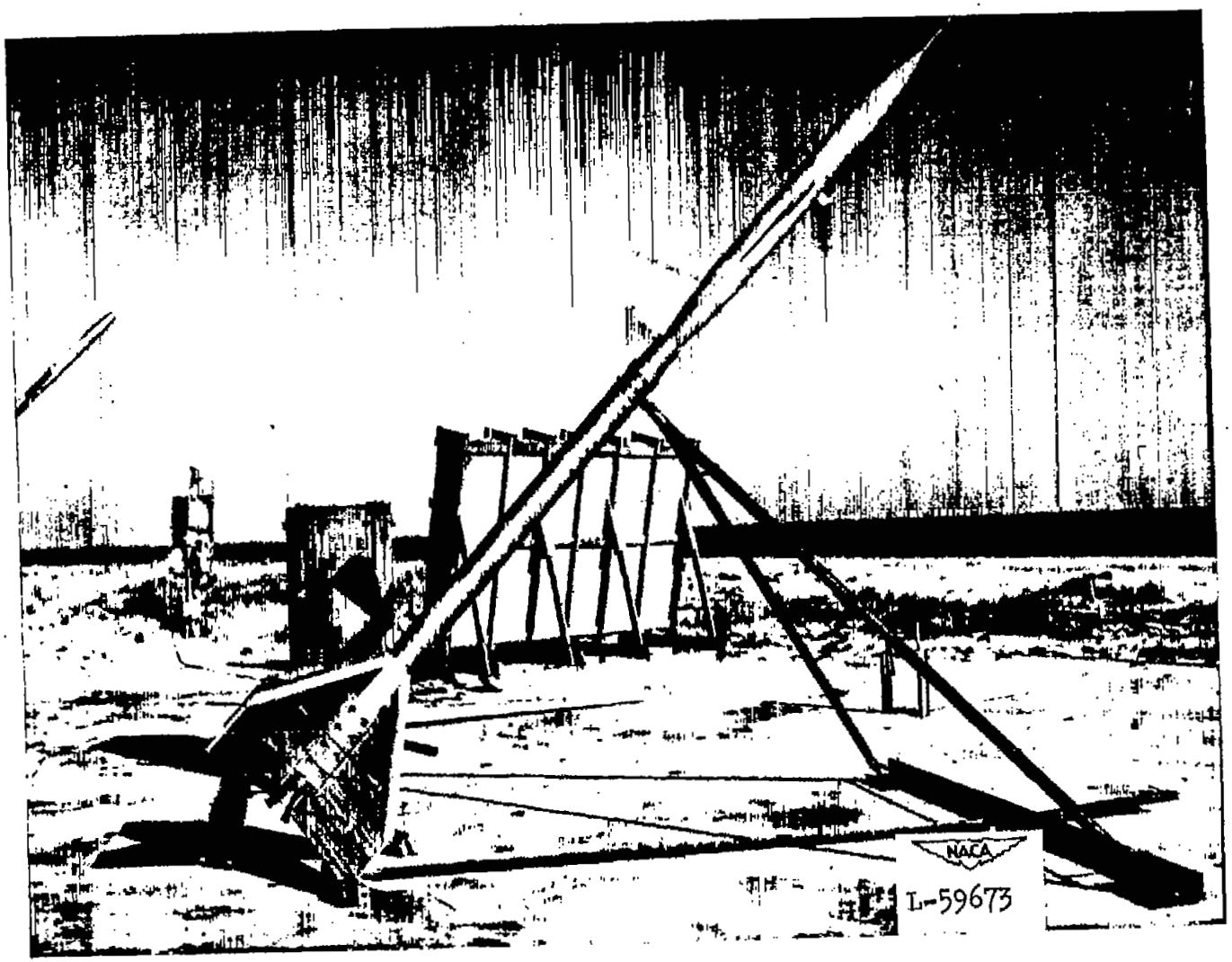

Figure 4.- Model on launcher.

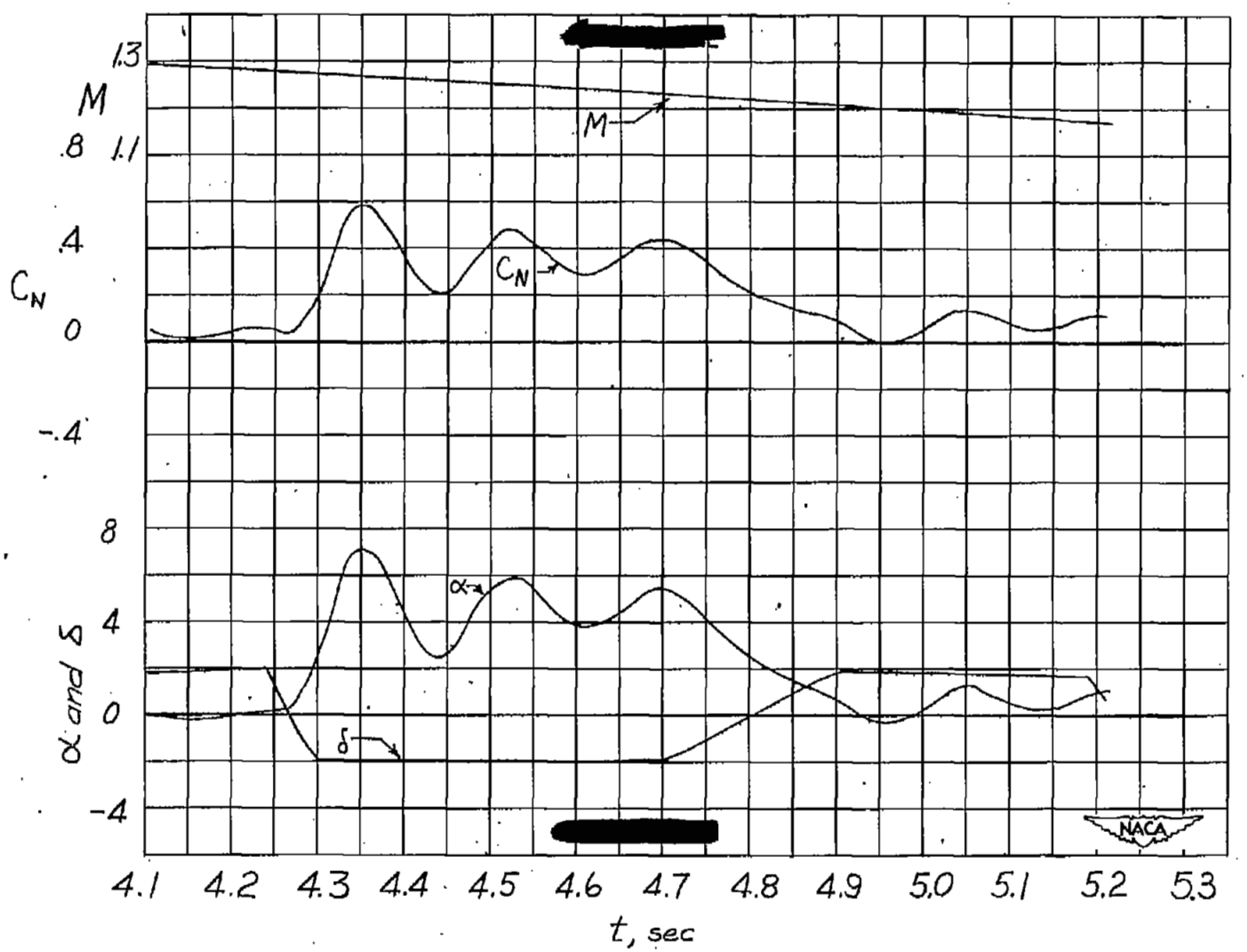

(a) Supersonic.

Figure 5.- Typical portions of time history of flight.

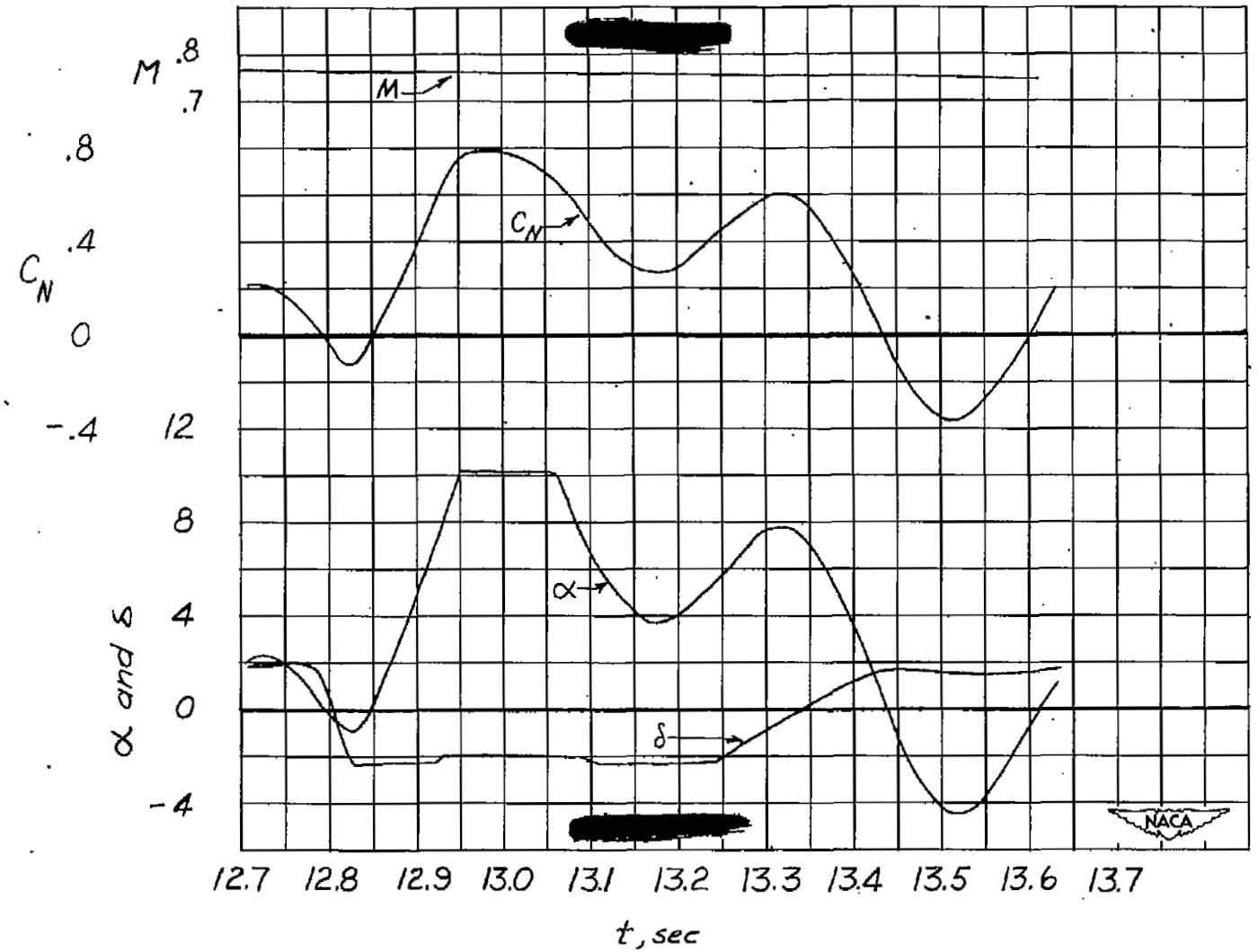

(b) Subsonic.

Figure 5.- Concluded.

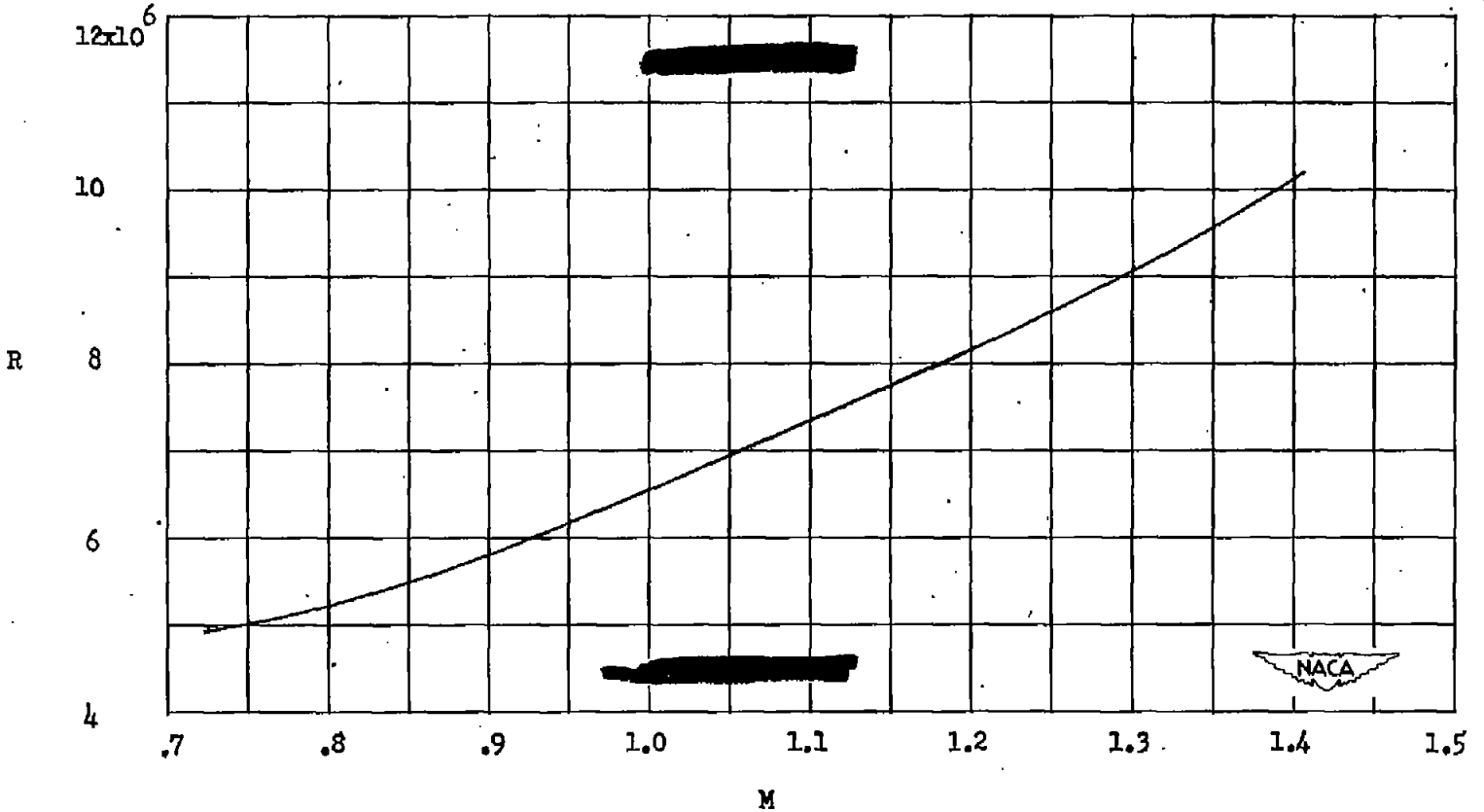

Figure 6.- Scale of test.

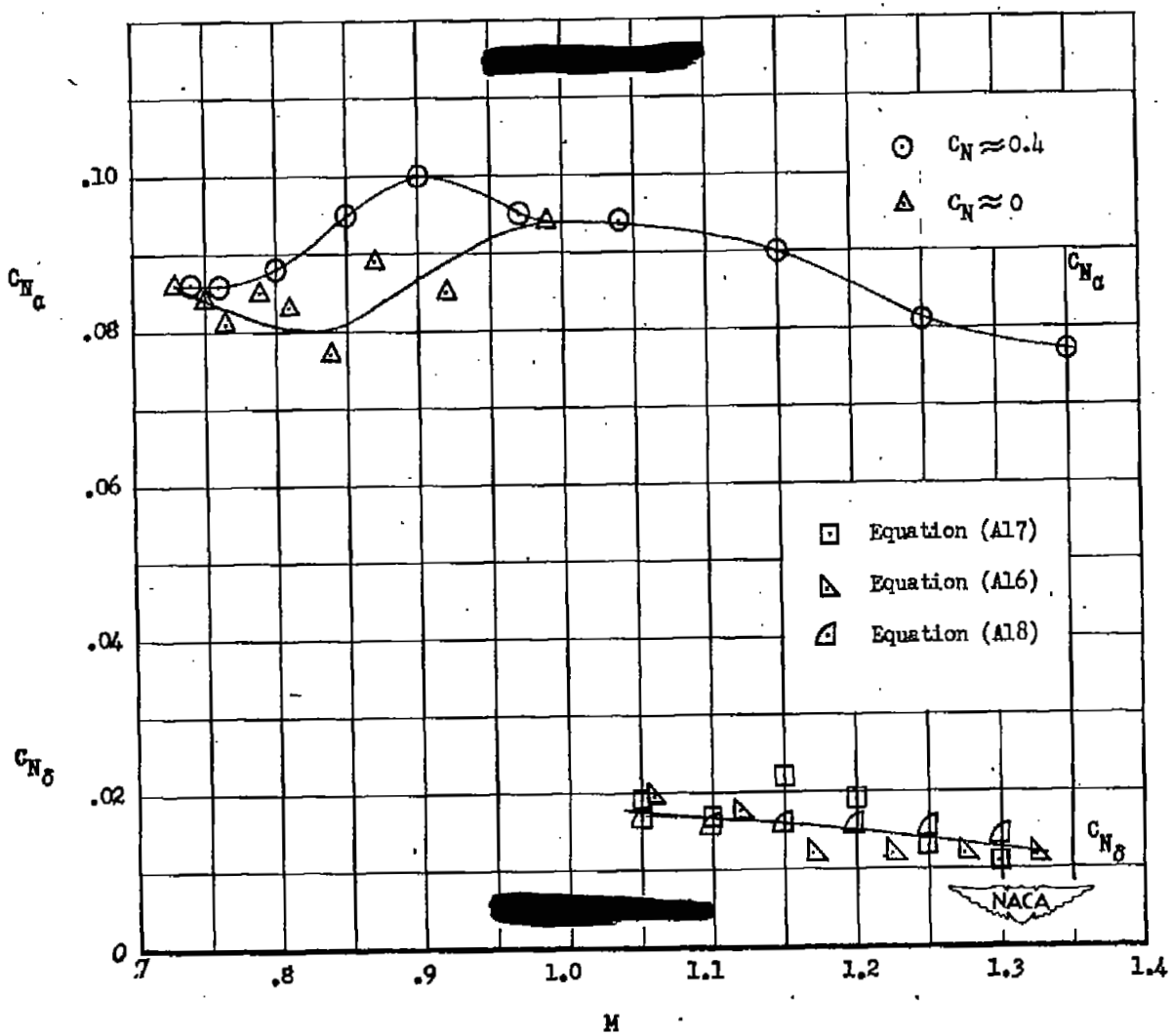

Figure 7.- Lift-curve slopes.

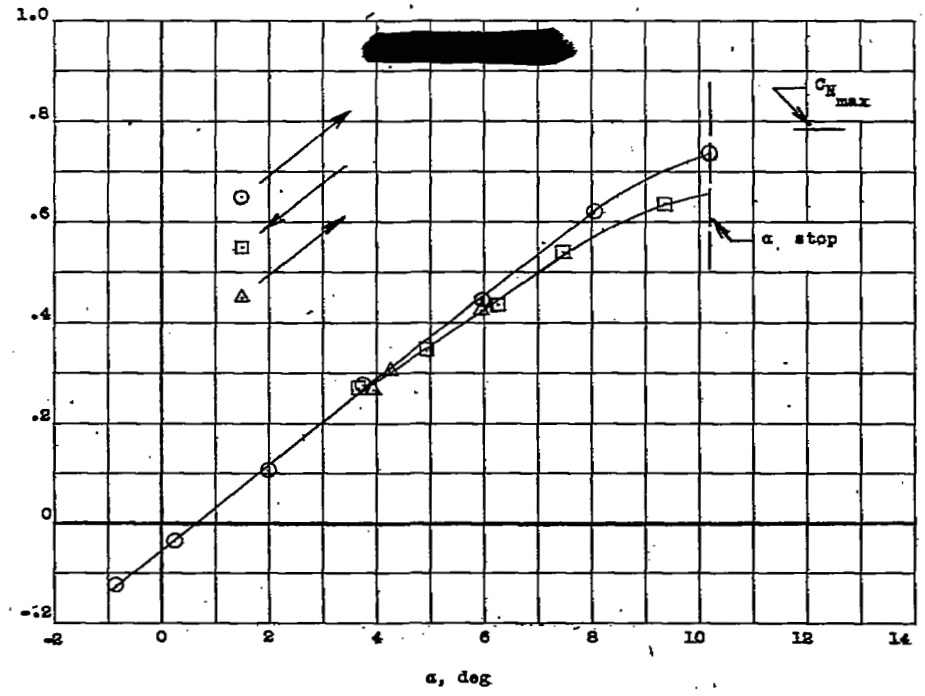

(a) M = 0.76.

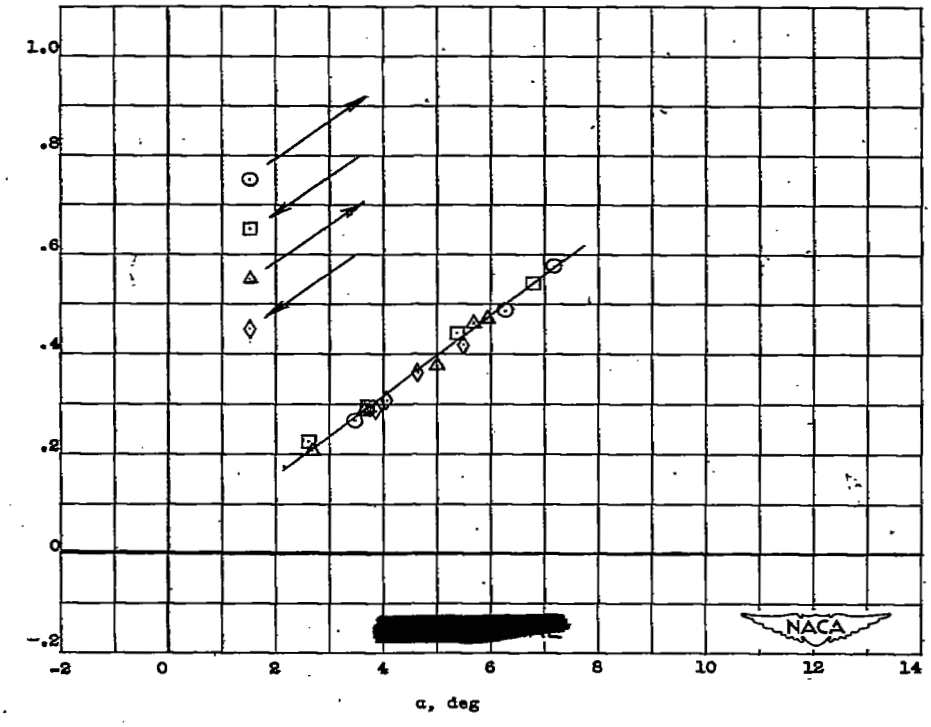

(b) M = 1.25.

Figure 8.- Variation of normal-force coefficient with angle of attack. Arrows indicate direction of angle-of-attack variation during oscillation.

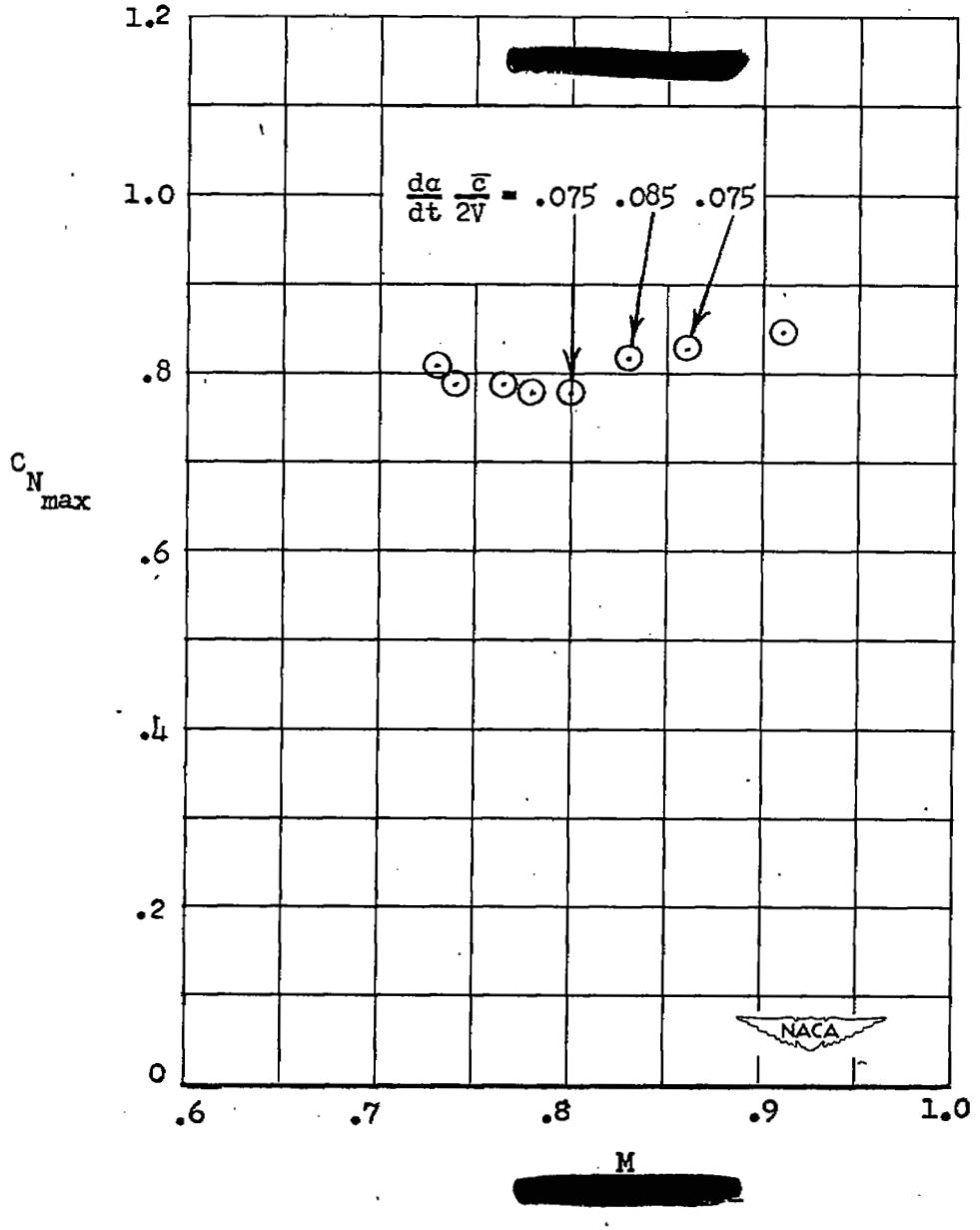

Figure 9.- Maximum normal-force coefficients obtained in region where model apparently stalled.

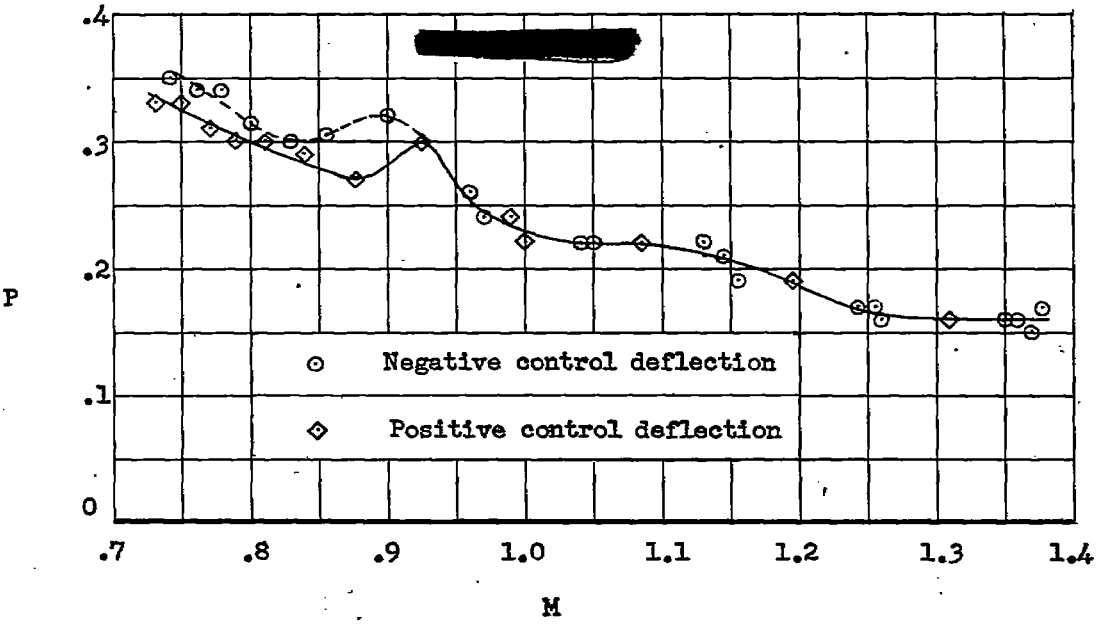

(a) Period of oscillation.

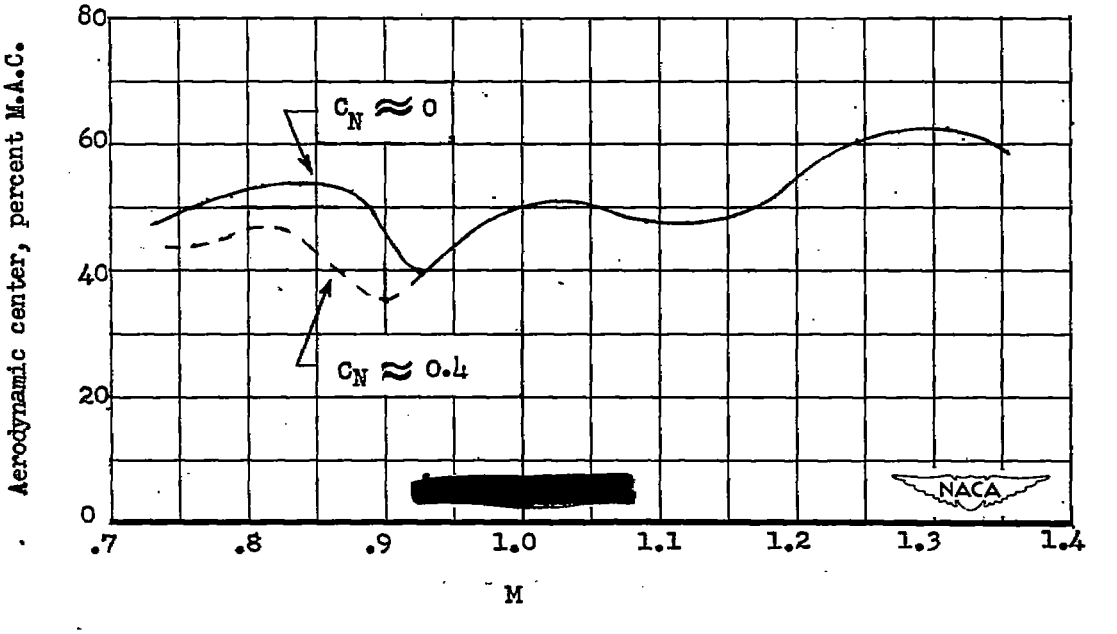

(b) Aerodynamic-center location.

Figure 10.- Static stability characteristics.

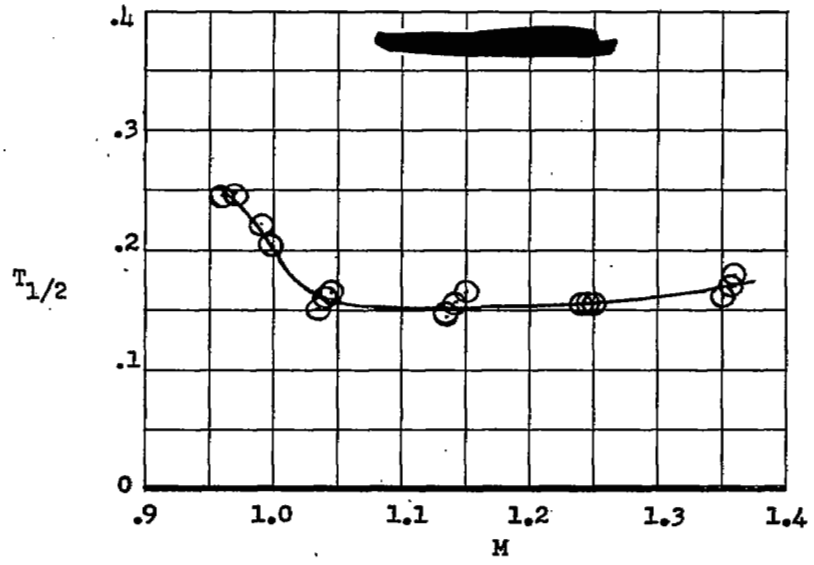

(a) Time to damp to one-half amplitude.

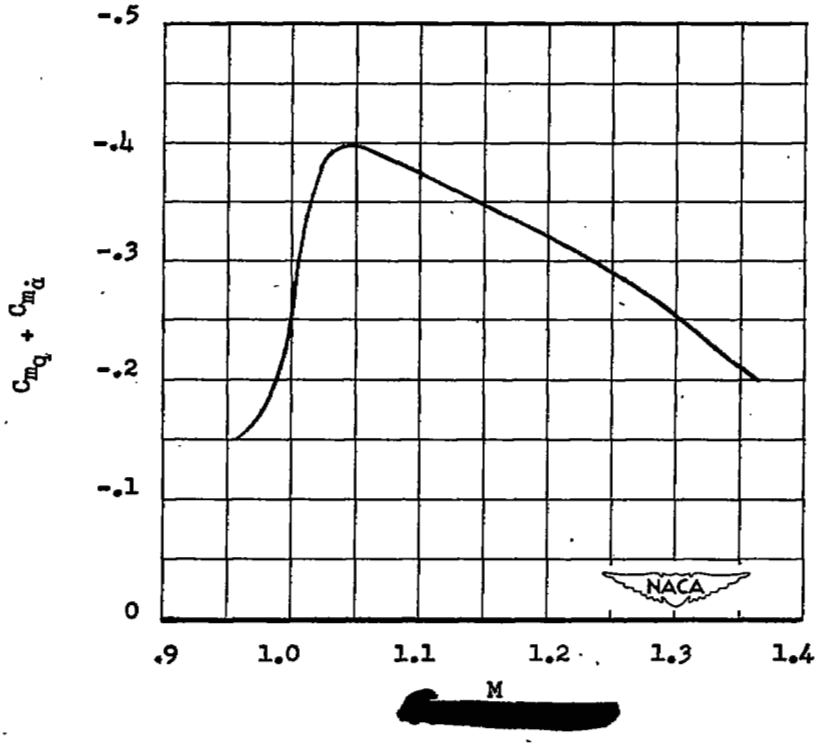

(b) Damping factor $\left(C_{m_q} + C_{m_{\dot{\alpha}}} \right)$.

Figure 11.- Damping characteristics of short-period oscillation.

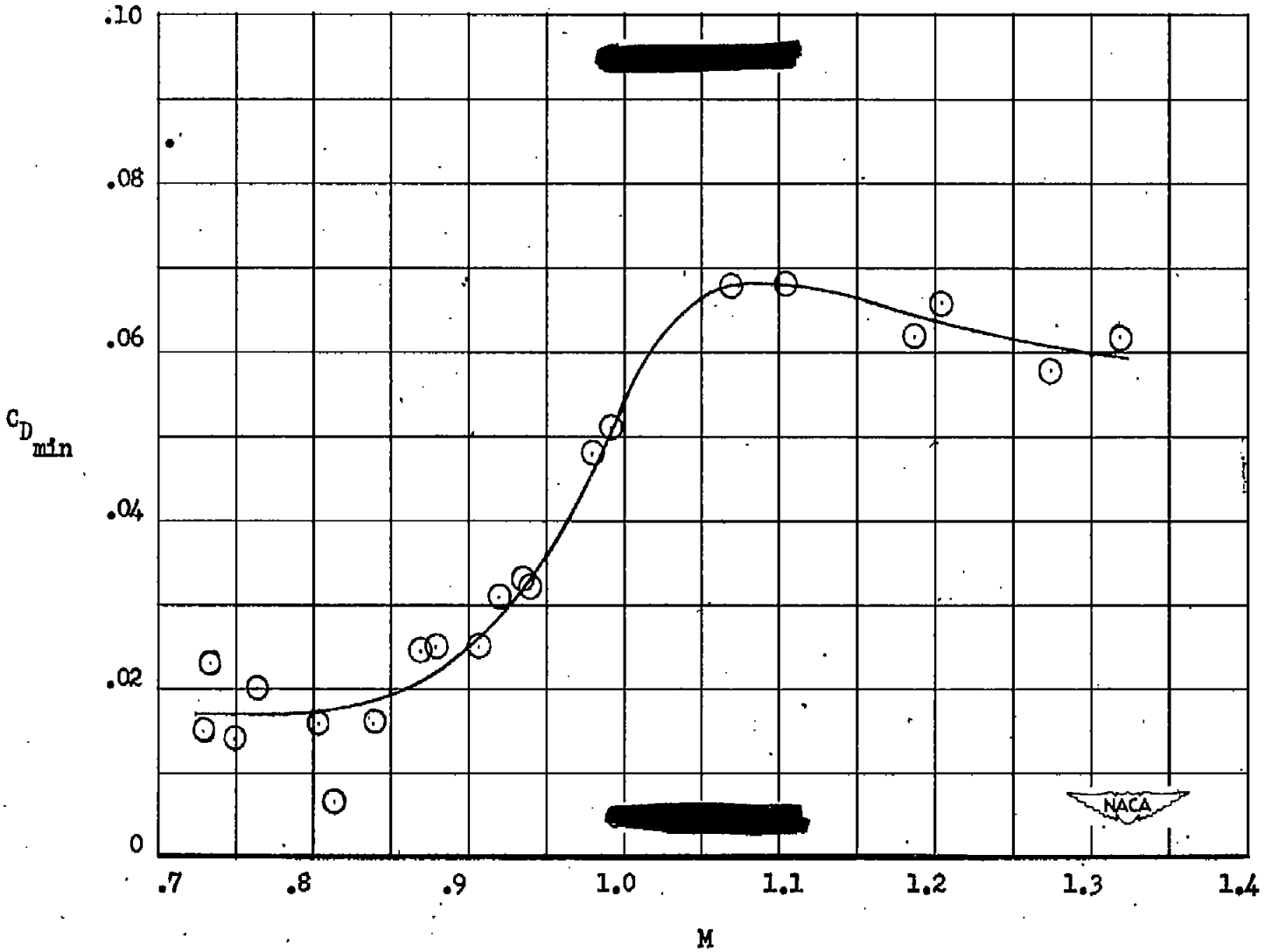

Figure 12.- Variation of minimum drag coefficients with Mach number.

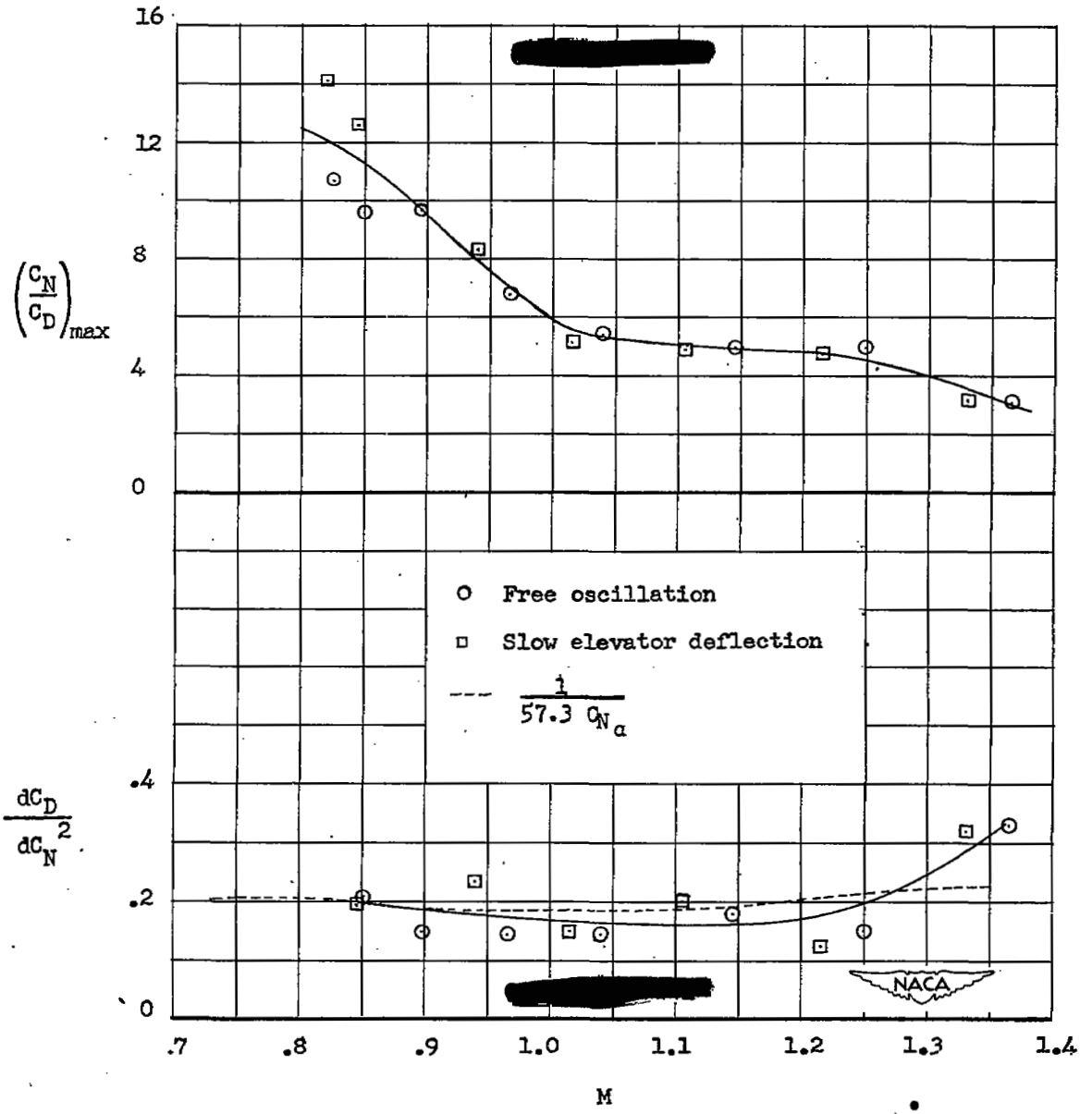

Figure 13.- Effect of lift on drag.

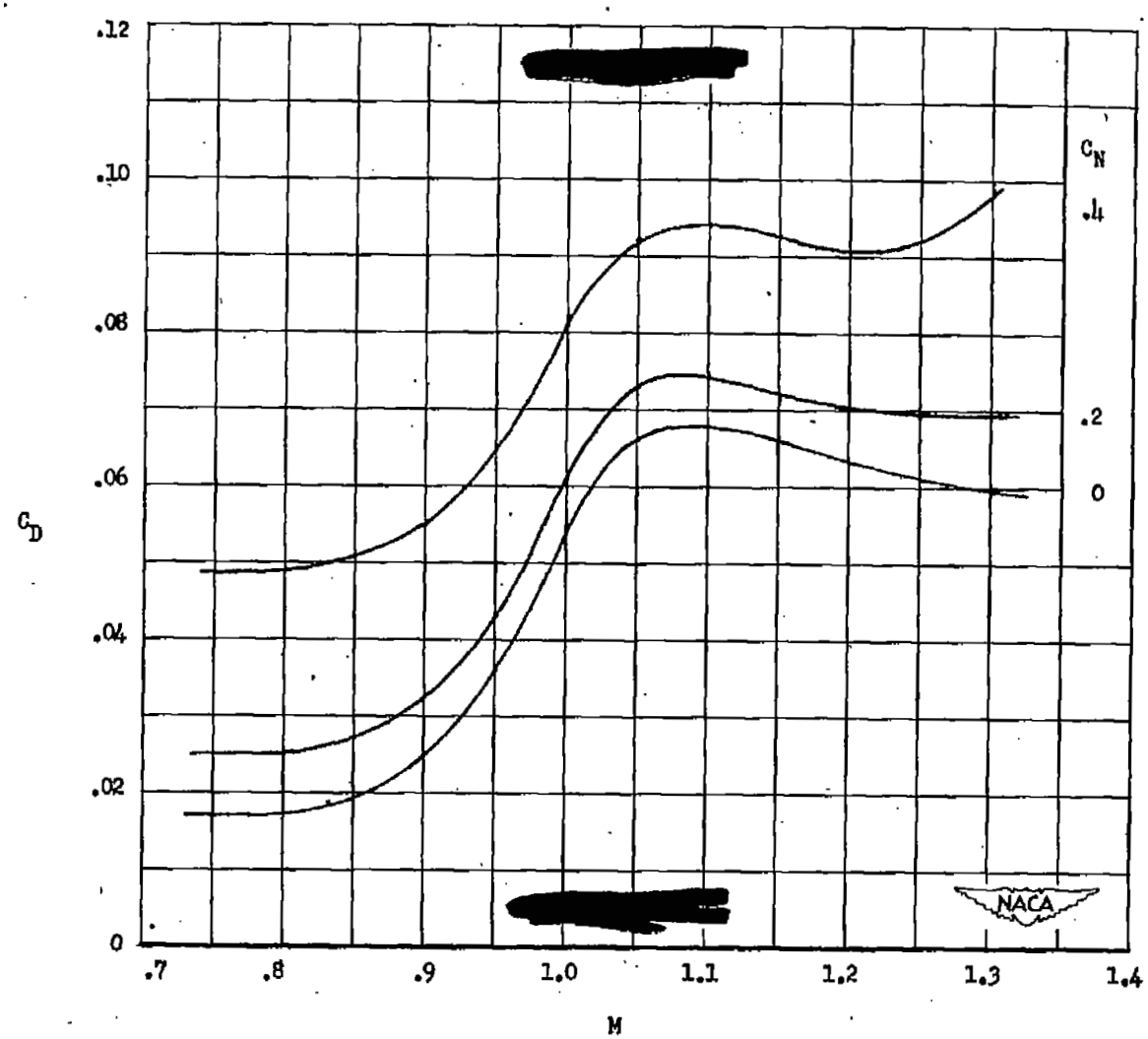

Figure 14.- Variation of drag with Mach number and normal-force coefficient.

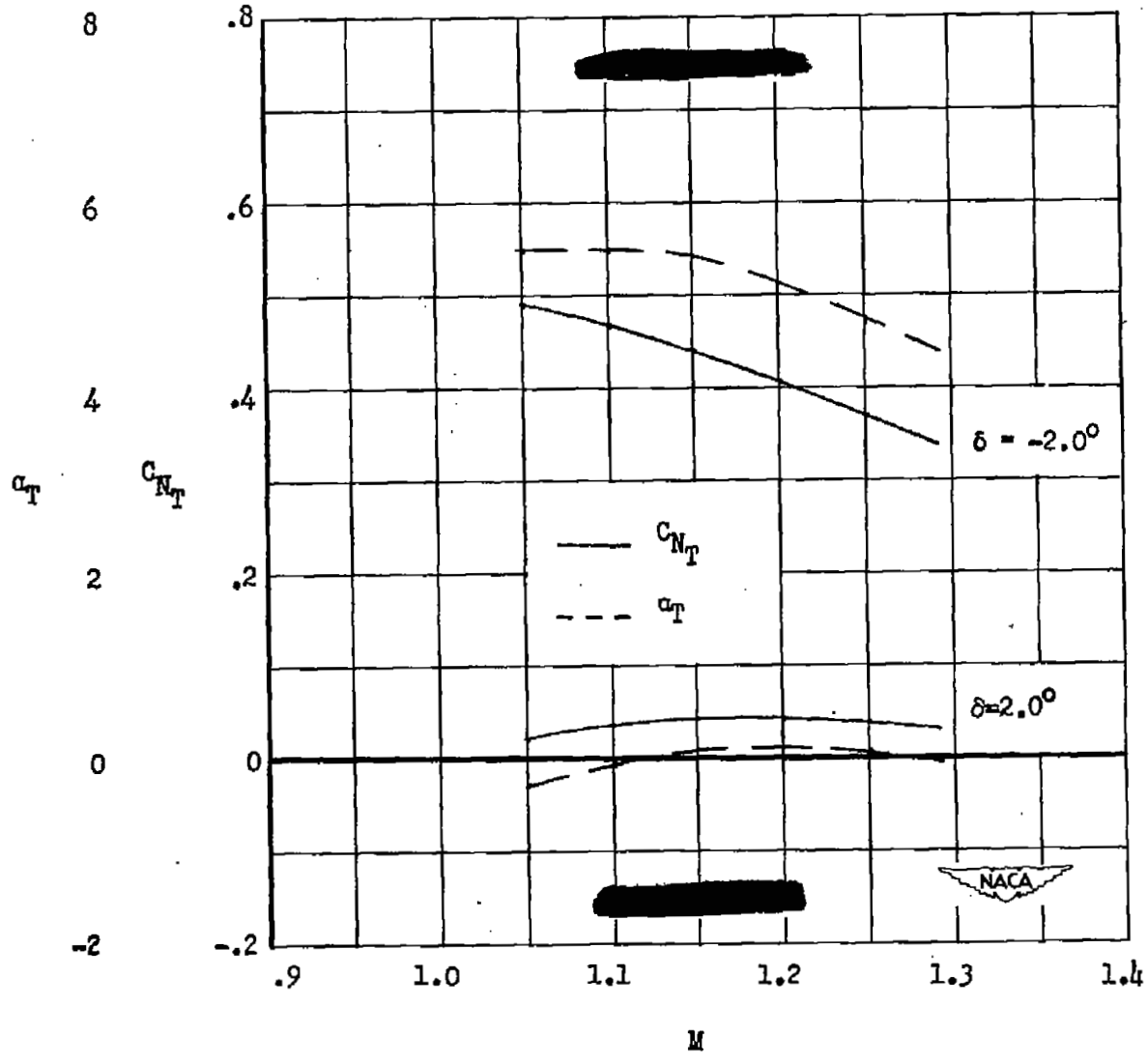

Figure 15.- Variation of trim normal-force coefficients and angles of attack with Mach number.

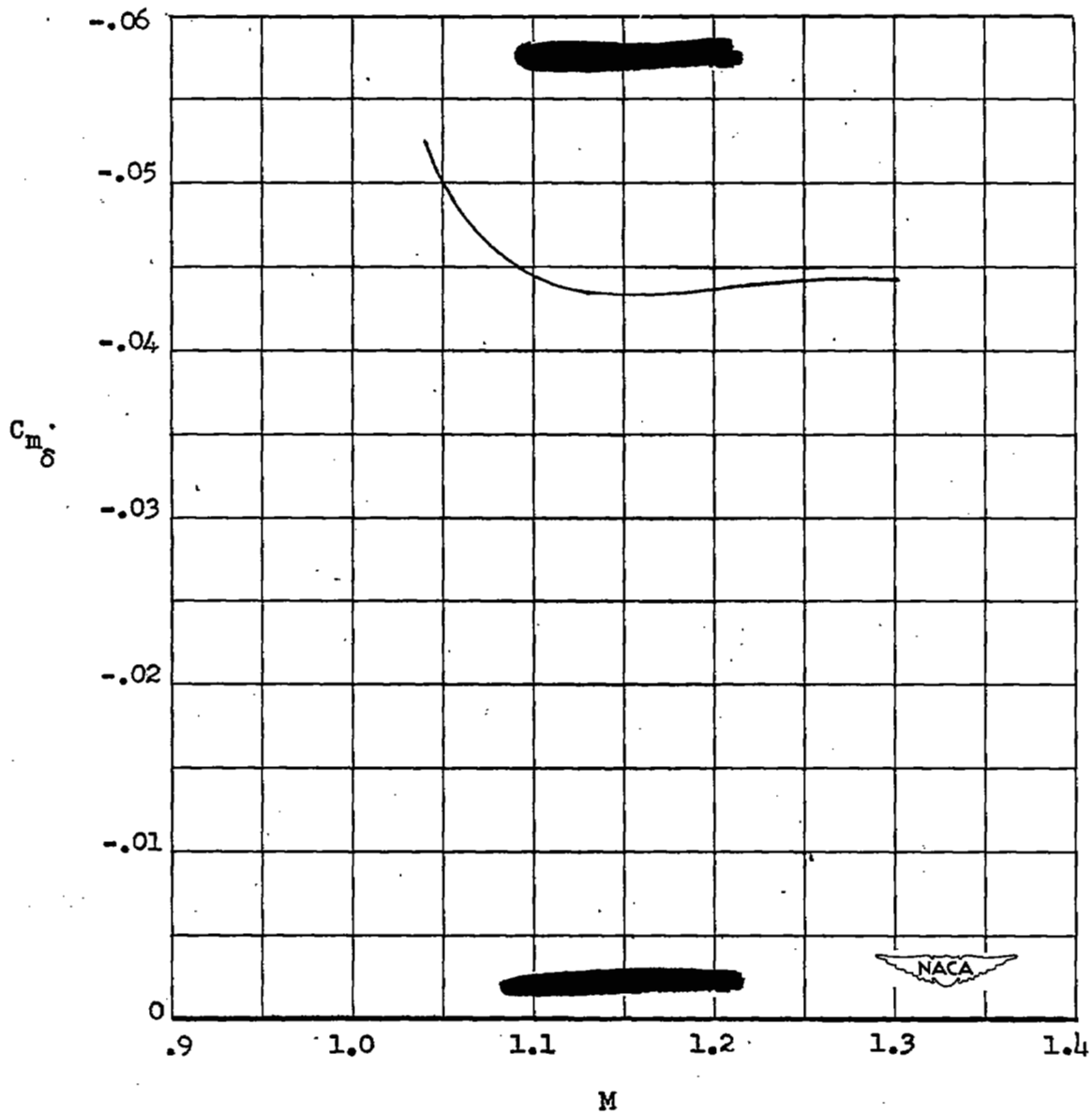

Figure 16.- Effectiveness of the elevator in producing pitching moment.

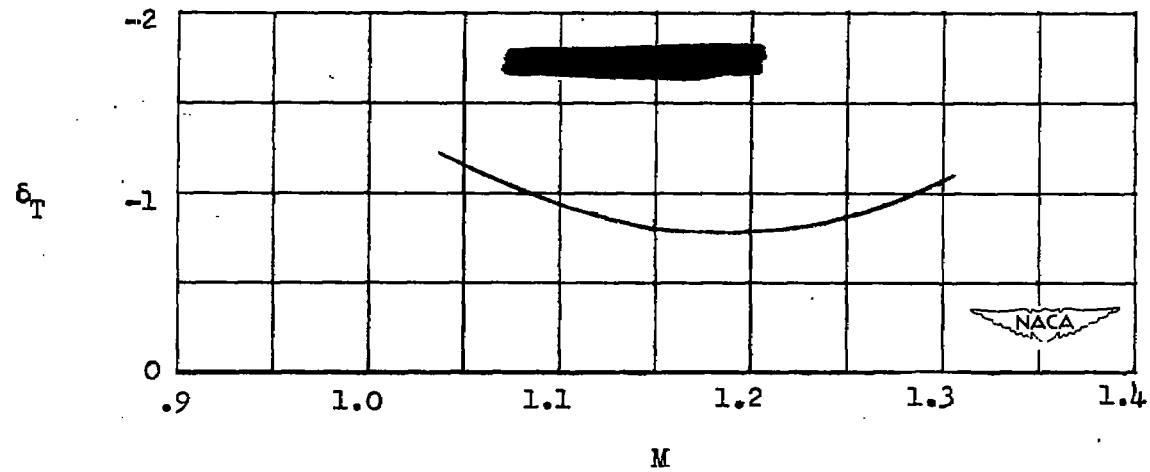

Figure 17.- Elevator deflection for level flight for assumed airplane at 40,000 feet.

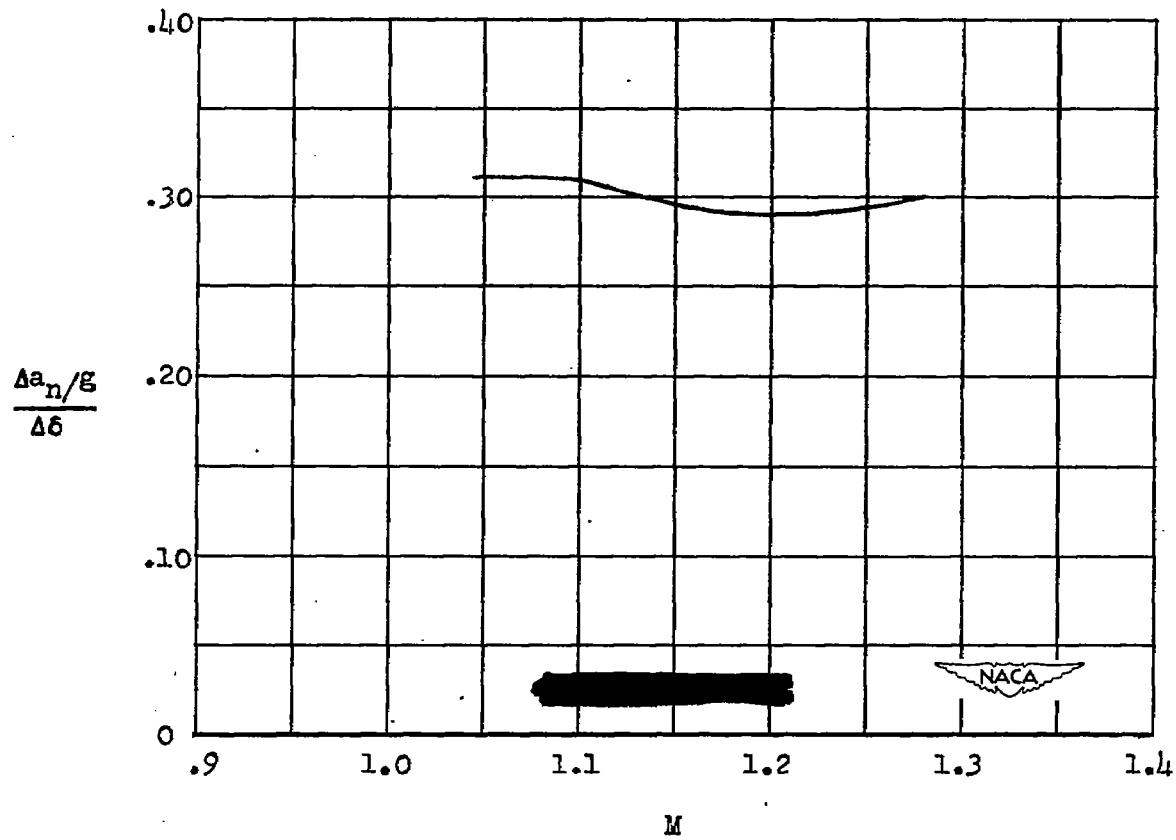

Figure 18.- Elevator effectiveness for assumed airplane at 40,000 feet.

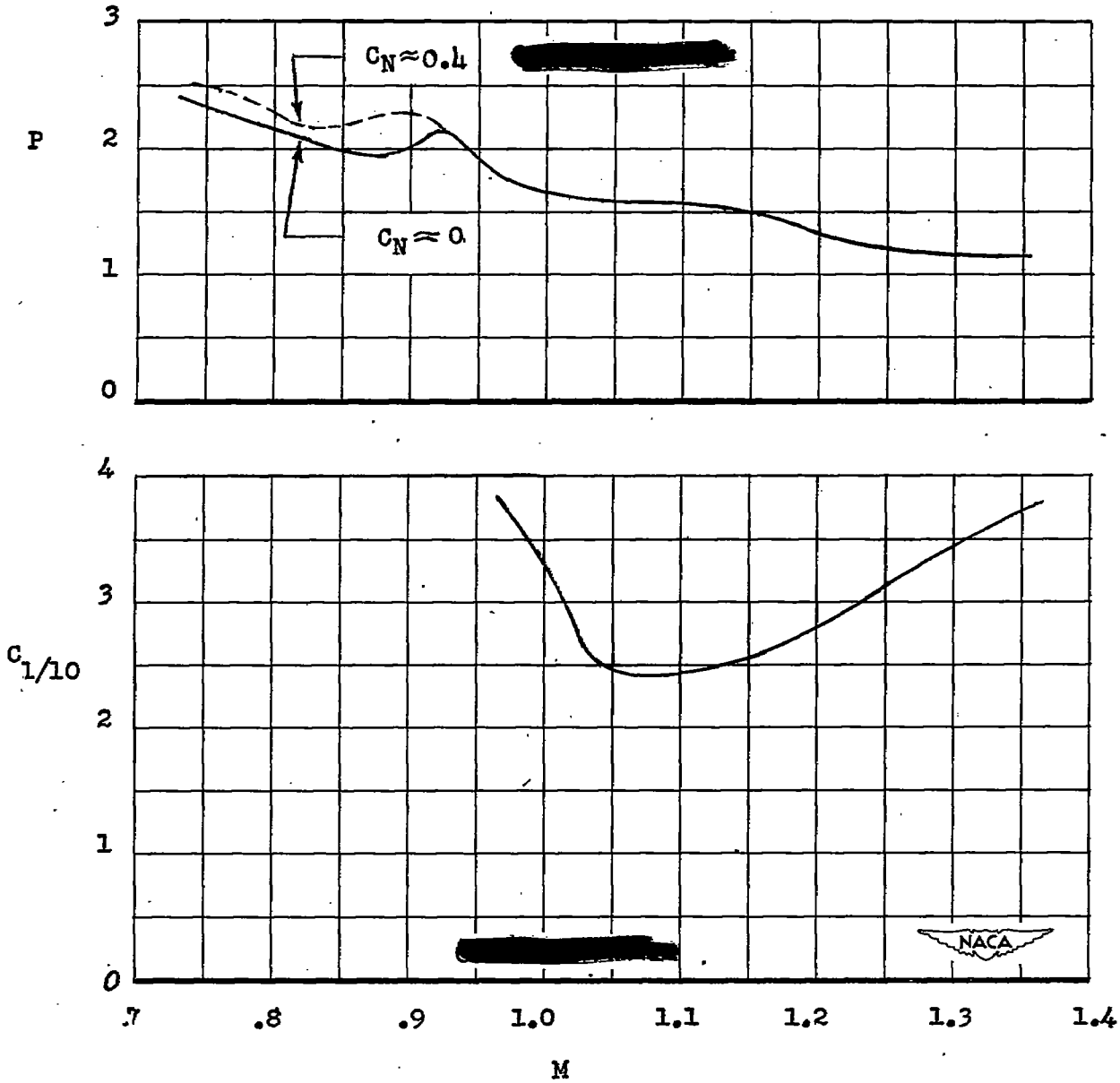

Figure 19.- Characteristics of short-period longitudinal oscillation for assumed airplane. Altitude, 40,000 feet.

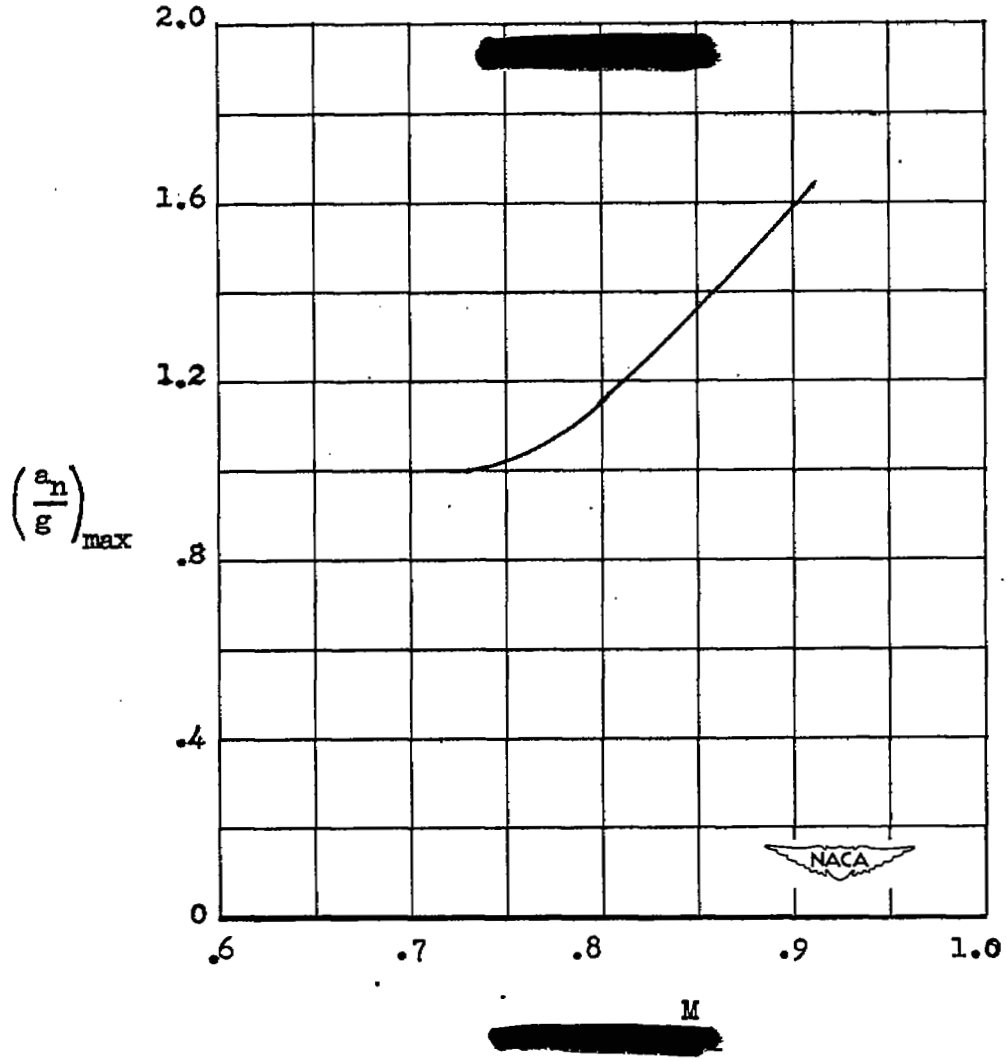

Figure 20.- Maximum normal acceleration for assumed airplane at 40,000 feet.

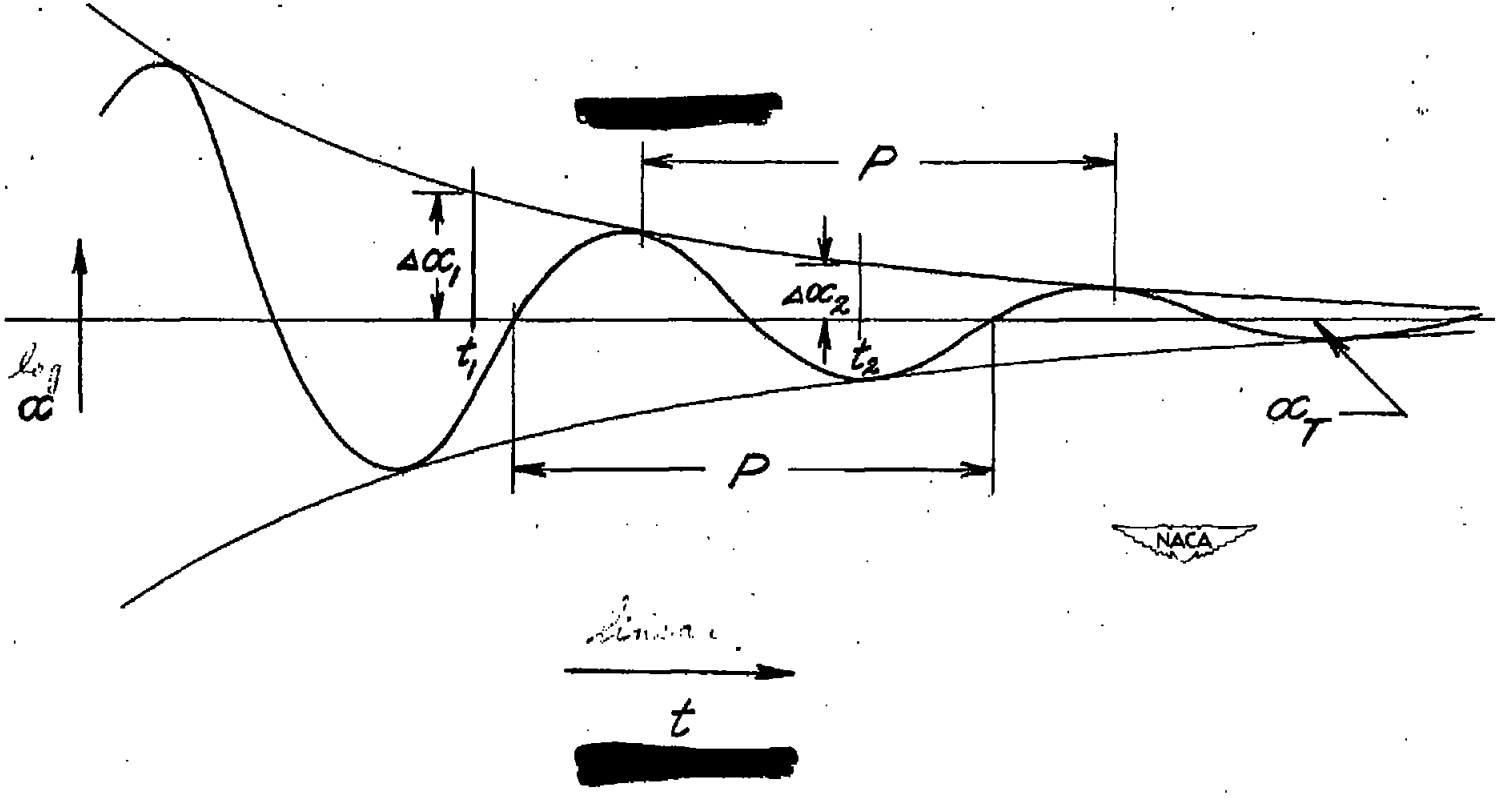

Figure 21.- Typical angle-of-attack oscillation as used in analysis.